SCATTERING IN BERNAL STACKED TRI-LAYER GRAPHENE

OZAIR SAEED

Supervisors:
Dr. C. Dutreix
Dr. E. A. Stepanov
June 2016

ABSTRACT

In this thesis we characterize multi-layer graphene within the tight-binding model and compute the low energy band structure to reveal the nature of particles situated at the Dirac points. We also address the problem of scattering through a localized impurity located on the surface of a tri-layer graphene system and focus on the modulations it induces on the two surfaces. We approach this problem within the framework of a T-matrix formalism, both numerically and analytically, which encases all possible scattering events thus enabling a realistic description of impurity scattering. We find that the impurity induces Friedel oscillations that decay with $\frac{1}{r}$ in graphene with more than one layer. The modulations are then analyzed in momentum space where we find that Bernal (ABA) stacked tri-layer graphene has specific characteristics that allow it to be distinguished from rhombohedral (ABC) tri-layer graphene. Experimentally these properties can be imaged directly from scanning tunneling microscopy.

ACKNOWLEDGMENTS

Writing a thesis is hard work and I could not have done it alone. Therefore I would like to express my gratitude to my supervisors dr. Clement Dutreix and dr. Zhenya Stepanov for answering my questions and teaching me how to numerically model systems. I learned a lot in the past few months. I would also like to thank prof. dr. Misha Katsnelson for providing me with the opportunity to do my thesis in his department.

CONTENTS

LIST OF FIGURES

INTRODUCTION

1.1 INTRODUCTION TO GRAPHENE

Carbon is a peculiar element, it has many allotropes which have a wide range of properties. Graphite, by far the most common allotrope, is an incredible soft and opaque substance and an excellent dry lubricant, an electrical conductor and a thermal insulator. Diamond on the other hand is the hardest natural occurring material, transparent, an electrical insulator and a thermal conductor. There are several more allotropes of carbon including but not limited to fullerenes, amorphous carbon, glassy carbon and graphene. Graphene (and its related fullerenes) particularly has been in the limelight for quite some time, being the first isolated 2D material in 2004 by A. K. Geim and K. S. Novoselov[1]. They ultimately received the Nobel prize for their work in 2010. Before its isolation in 2004 single layers of graphite were already under consideration since the 1940's [2] which were thought to be unstable at non-zero temperature according to the Mermin-Wagner theorem causing thermal fluctuations to destroy any long range order in the lattice. Yet graphene is stable due to intrinsic ripples in the lattice which effectively cancel out the thermal fluctuations at long range [3].

Graphene is light and yet immensely strong due to its carbon-carbon bonds, additionally graphene also has elastic properties, being able to retain its initial size after strain. But what makes graphene really special are its electronic properties. Graphene is a zero-overlap semimetal with a linear energy spectrum resulting in massless quasi-particles near the Dirac points which are located at the six corners of the Brillouin zone. These quasi-particles behave like relativistic particles near these Dirac points[4, 5] and are described by a 2D Dirac equation instead of the Schrodinger equation hence the quasi-particles are also called massless Dirac fermions. From this arise a number of effects such as Klein tunneling. Because graphene has sp^2 hybridised orbitals meaning each carbon atom uses three of its four available electrons to bond with neighbouring atoms and the leftover electron is free to move along the plane. This makes graphene an excellent electrical conductor unlike for example diamond which has sp^3 hybridised orbitals meaning all available electrons form bonds with neighbouring atoms.

To measure a material's properties experimentally one often uses a scanning tunneling microscope (STM) to probe the surface. This way an image can be built of the surface. When electrons scatter from an impurity they produce modulations in the local density of states which can then be measured with STM.

These facts make graphene an interesting candidate for semi-conductor research, possibly lending itself to revolutionising micro- and computer-technology.

In the following chapters we first describe graphene in the tight binding model. From this we will build bi-layer and tri-layer graphene in two different configurations and illustrate

their full and low energy band structure. Then we will describe the transfer matrix formalism in which we will discuss the Green functions and how to get the local density of states in this formalism. Afterwards we will illustrate the local density of states in both real space and momentum space for tri-layer graphene and discuss its features.

TIGHT-BINDING GRAPHENE MODEL

2.1 SINGLE LAYER GRAPHENE

Graphite is a material that has been in use for centuries. It consists of layers of carbon atoms arranged on a honeycomb lattice. Each of these layers is bound to each other by the Van der Waals force. A single layer of graphite is called graphene because graphene is only one atom thick it differs quite a bit from graphite.

A lattice is referred to as a Bravais lattice when it is an infinite array of discrete points with an arrangement and orientation that appears exactly the same, from whichever of the points the array is viewed [6]. Graphene's crystal lattice is displayed in Fig. 2.1, from this it becomes quite clear that graphene's crystal lattice is not a Bravais lattice because only the next-nearest neighbours have an equivalent surrounding. Therefore we can identify two hexagonal Bravais sublattices A and B which form graphene's lattice which are shifted relatively to each other by the carbon-carbon distance of $a \approx 1.42$Å. To express this more formally we identify the primitive vectors with which a sublattice can be constructed:

$$\vec{a_1} = \frac{3a}{2} \begin{bmatrix} \frac{1}{\sqrt{3}} \\ 1 \end{bmatrix} \qquad\qquad \vec{a_2} = \frac{3a}{2} \begin{bmatrix} -\frac{1}{\sqrt{3}} \\ 1 \end{bmatrix} \tag{2.1}$$

Each carbon atom has three nearest neighbours whose position can be identified with the three vectors $\vec{\delta_1}$, $\vec{\delta_2}$ and $\vec{\delta_3}$:

$$\vec{\delta_1} = \frac{a}{2}\left(\sqrt{3}, 1\right) \qquad \vec{\delta_2} = \frac{a}{2}\left(-\sqrt{3}, 1\right) \qquad \vec{\delta_3} = (0, -a) \tag{2.2}$$
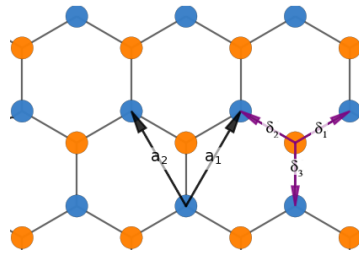
Figure 2.1: Part of graphene's honeycomb lattice consisting of two sublattices A (blue dot) and B (orange dot). The two primitive vectors $\vec{a_1}$ and $\vec{a_2}$ and the three nearest neighbour vectors $\vec{\delta_1}$, $\vec{\delta_2}$ and $\vec{\delta_3}$. The unit cell can be taken as the inner part of a hexagon with each atom contributing $\frac{1}{3}$ of an atom making it have 2 atoms per unit cell. Note that although the sublattices are not equivalent they are both carbon atoms.

We can therefore describe each complete sublattice by

$$R_A = n_1 \vec{a_1} + n_2 \vec{a_2} \tag{2.3}$$
$$R_B = n_1 \vec{a_1} + n_2 \vec{a_2} + \vec{e_B} \tag{2.4}$$

where $\vec{e_B} = \begin{bmatrix} 0 \\ a \end{bmatrix}$ and $n_1, n_2 \in \mathbb{Z}$. Then the entire non-Bravais lattice is described by

$$R = R_A \oplus R_B \tag{2.5}$$

Based upon Eq. (2.5) we can classify graphene belonging to the group of bipartite lattices. Therefore graphene is a bipartite non-Bravais lattice with two atoms per unit cell.

2.2 THE RECIPROCAL LATTICE

It is interesting to look at the reciprocal lattice. The reciprocal lattice can be obtained by Fourier transforming the lattice in figure 2.1 as a result the reciprocal lattice is in momentum space instead of real space. In the same way that the real space lattice can be constructed with two primitive vectors the reciprocal lattice can also be constructed with two reciprocal primitive vectors $\vec{b_1}$ and $\vec{b_2}$ which can be computed with the Laue condition $\vec{a_i} \cdot \vec{b_j} = 2\pi\delta_{ij}$ where δ_{ij} is the usual Kronecker delta and $i, j \in 1, 2$:

$$\vec{b_1} = \frac{2\pi}{3a} \begin{bmatrix} 1 \\ \sqrt{3} \end{bmatrix} \qquad\qquad \vec{b_2} = \frac{2\pi}{3a} \begin{bmatrix} -1 \\ \sqrt{3} \end{bmatrix} \tag{2.6}$$

In Fig. 2.2 the first Brillouin zone is depicted together with the primitive vectors from Eq. (2.6). We see that the first Brillouin zone again forms a hexagon but rotated by $\frac{\pi}{2}$ compared to the lattice in real space. Because free electrons in an infinite crystal are described by Bloch wavefunctions that have crystal periodicity. Therefore the corresponding wavefunctions in momentum space only differ in phase from the first Brillouin zone and we can shift all momenta inside of the first Brillouin zone. In the low energy regime this narrows down even further to just the corners of the Brillouin zone which are given by [7]

$$K_{mn}^{\pm} = \pm\frac{\vec{b_1} - \vec{b_2}}{3} + m\vec{b_1} + n\vec{b_2} \tag{2.7}$$

Only two corners are non-equivalent, meaning they can't be connected via the reciprocal vectors, which we shall define as K and K_2

$$K = \frac{4\pi}{\sqrt{3}a} \begin{bmatrix} \frac{1}{\sqrt{3}} \\ 0 \end{bmatrix} \qquad\qquad K_2 = \frac{4\pi}{\sqrt{3}a} \begin{bmatrix} \frac{\sqrt{3}}{6} \\ \frac{1}{2} \end{bmatrix} \tag{2.8}$$
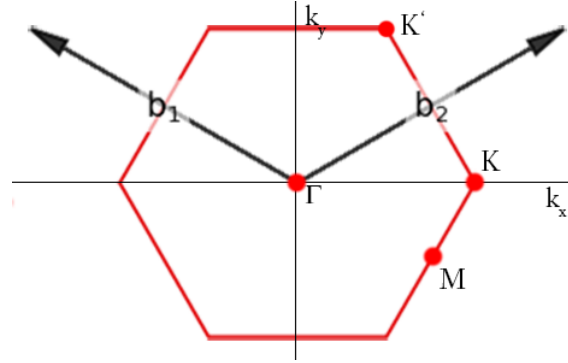
Figure 2.2: The first Brillouin zone together with the points M, Γ, K and K′.

2.3 ELECTRON CREATION AND ANNIHILATION OPERATORS

Every carbon atom in the graphene lattice uses three of its four electrons to form bonds to neighbouring carbon atoms, the fourth electron is free to move through the lattice. To describe these free electrons we use the tight-binding model under a second quantization formalism. The atoms in the lattice can be regarded as a periodic attractive potential at every atom. The free electrons feel an attractive force towards said atoms and tunnel from atom to atom. In the tight-binding model the tunnelling effect is described as hoppings between the carbon atoms. Of course the electrons are not really free with respect to the potential induced by the atoms but rather they are quasi-free electrons

We start by introducing a set of new operators. The creation operator $\hat{c}_{\vec{j},\sigma}^{\dagger}$ creates an electron at lattice site $\vec{j}$ with spin σ while the annihilation operator $\hat{c}_{\vec{i},\sigma}$ annihilates an electron at site $\vec{i}$. Since we're talking about electrons the spin can only take two values $\sigma = \pm\frac{1}{2} = \uparrow, \downarrow$ and are also subject to the Pauli exclusion principle, no two electrons can be in the same state. To formalize this we introduce the anti-commutation relations

$$\left\{\hat{c}_{\vec{j},\sigma}, \hat{c}_{\vec{i},\sigma'}^{\dagger}\right\} = \delta_{\vec{j},\vec{i}}\delta_{\sigma,\sigma'} \tag{2.9}$$

$$\left\{\hat{c}_{\vec{j},\sigma}^{\dagger}, \hat{c}_{\vec{i},\sigma'}^{\dagger}\right\} = 0 \tag{2.10}$$

$$\left\{\hat{c}_{\vec{j},\sigma}, \hat{c}_{\vec{i},\sigma'}\right\} = 0 \tag{2.11}$$

where the anti-commutator of two operators is defined as

$$\left\{\hat{A}, \hat{B}\right\} = \hat{A}\hat{B} + \hat{B}\hat{A} \tag{2.12}$$

We see that the Pauli exclusion principle is obeyed by trying to create or annihilate two electrons of the same spin on the same site and using the the anti-commutation relations in Eq. (2.10) and Eq. (2.11)

$$c_{\vec{j},\sigma}^{\dagger 2} = \frac{1}{2}\left\{\hat{c}_{\vec{j},\sigma}^{\dagger}, \hat{c}_{\vec{i},\sigma'}^{\dagger}\right\} = 0 \tag{2.13}$$

$$c_{\vec{j},\sigma}^{2} = \frac{1}{2}\left\{\hat{c}_{\vec{j},\sigma}, \hat{c}_{\vec{i},\sigma'}\right\} = 0 \tag{2.14}$$

The product of both operators summed over the spins gives the occupation number $n_{\vec{j}}$ for the number of electrons at site $\vec{j}$ and by extension summing the occupation number over all lattice sites gives us the total number of free electrons in the lattice

$$n_{\vec{j}} = \sum_{\sigma} \hat{c}_{\vec{j}}^{\dagger}\hat{c}_{\vec{j}} \tag{2.15}$$

$$N = \sum_{\vec{j}} n_{\vec{j}} \tag{2.16}$$

Every state can now be made by a combination of creation operators working upon the vacuum state $|0\rangle$

$$|\psi\rangle = \prod_{\vec{j}} \left(\hat{c}_{\vec{j},\uparrow}^{\dagger}\right)^{n_{\vec{j},\uparrow}} \left(\hat{c}_{\vec{j},\downarrow}^{\dagger}\right)^{n_{\vec{j},\downarrow}} |0\rangle \tag{2.17}$$

where due to the system being fermionic the occupation number $n_{\vec{j},\uparrow}$ or $n_{\vec{j},\downarrow}$ can only take values of 0 and 1. Thus each site can be empty or occupied by a fermion with spin up or with spin down or by two fermions with opposite spin.

2.4 NEAREST NEIGHBOUR HOPPING

To describe the band structure of graphene we consider one electron at each lattice site and allow them to hop to any nearest neighbouring site i.e. the sites characterised by Eq. (2.2). We shall neglect any interaction between the electrons themselves or interaction between the electrons and the atoms and solely focus on the tunnelling effects between neighbouring sites.

The Hamiltonian is then described by

$$H_0 = -t \sum_{\langle \vec{j},\vec{i}\rangle} \sum_{\sigma} \left(a_{\vec{j},\sigma}^{\dagger} b_{\vec{i},\sigma} + b_{\vec{j},\sigma}^{\dagger} a_{\vec{i},\sigma}\right) \tag{2.18}$$

where the creation and annihilation for sublattice A and B were introduced as $a_{\vec{j},\sigma}^{\dagger}$, $a_{\vec{j},\sigma}$ and $b_{\vec{j},\sigma}^{\dagger}$, $b_{\vec{j},\sigma}$, the intralayer hopping parameter t which defines the tunnelling amplitude and the sum runs over all nearest neighbours $\vec{j}$ and $\vec{i}$ and spins up and down. The intralayer hopping parameter has an experimental value of about 2.8 [eV] [8]. We see that the Hamiltonian describes a creation of an electron with spin σ at sublattice A at position $\vec{j}$ and

destruction at sublattice B at position $\vec{\imath}$ and vice versa. To further simplify this we assume the electrons to be spinless so we can drop the summation over the spins which results in

$$H_0 = -t \sum_{\langle \vec{\jmath}, \vec{\imath} \rangle} \left(a_{\vec{\jmath}}^{\dagger} b_{\vec{\imath}} + b_{\vec{\jmath}}^{\dagger} a_{\vec{\imath}} \right) \tag{2.19}$$

Note that this Hamiltonian is hermitian as required $\left(H_0 = H_0^{\dagger} \right)$.

Because our system is translationally invariant it is convenient to Fourier transform our Hamiltonian to momentum space which makes it diagonal to the index $\vec{k}$. We can then extract the dispersion relation $E\left(\vec{k} \right)$.

We define the Fourier transform of the creation and annihilation operators as

$$a_{\vec{k}}^{\dagger} = \frac{1}{\sqrt{\Omega}} \sum_{\vec{\jmath}} e^{-i\vec{k}\cdot\vec{\jmath}} a_{\vec{\jmath}}^{\dagger} \tag{2.20}$$

$$a_{\vec{k}} = \frac{1}{\sqrt{\Omega}} \sum_{\vec{\imath}} e^{i\vec{k}\cdot\vec{\imath}} a_{\vec{\imath}} \tag{2.21}$$

and similarly for sublattice B and where Ω represents the volume of the Brillouin zone $\Omega = \frac{8\pi^2}{\sqrt{3}a^2}$. Our Hamiltonian then becomes

$$
\begin{aligned}
H_0 &= -\frac{t}{\Omega} \sum_{\langle \vec{j}, \vec{i} \rangle} \sum_{\vec{k}, \vec{k}'} \left(e^{-i\vec{k}\cdot\vec{j}} a_{\vec{k}}^\dagger e^{i\vec{k}'\cdot\vec{i}} b_{\vec{k}'} + e^{-i\vec{k}'\cdot\vec{i}} b_{\vec{k}'}^\dagger e^{i\vec{k}\cdot\vec{j}} a_{\vec{k}} \right) \\
&= -\frac{t}{\Omega} \sum_{\vec{j}, \delta_i} \sum_{\vec{k}, \vec{k}'} \left(e^{-i\vec{k}\cdot\vec{j}} a_{\vec{k}}^\dagger e^{i\vec{k}'(\vec{j}+\delta_i)} b_{\vec{k}'} + e^{-i\vec{k}'\cdot(\vec{j}+\delta_i)} b_{\vec{k}'}^\dagger e^{i\vec{k}\cdot\vec{j}} a_{\vec{k}} \right) \\
&= -\frac{t}{\Omega} \sum_{\vec{j}, \delta_i} \sum_{\vec{k}, \vec{k}'} \left(e^{i\vec{k}'\cdot\delta_i} e^{i(\vec{k}'-\vec{k})\cdot\vec{j}} a_{\vec{k}}^\dagger b_{\vec{k}'} + e^{-i\vec{k}'\cdot\delta_i} e^{i(\vec{k}'-\vec{k})\cdot\vec{j}} b_{\vec{k}'}^\dagger a_{\vec{k}} \right) \\
&= -t \sum_{\delta_i} \sum_{\vec{k}, \vec{k}'} \left(e^{i\vec{k}'\cdot\delta_i} \underbrace{\left(\frac{1}{\Omega} \sum_{\vec{j}} e^{i(\vec{k}'-\vec{k})\cdot\vec{j}} \right)}_{\delta_{\vec{k}, \vec{k}'}} a_{\vec{k}}^\dagger b_{\vec{k}'} + e^{-i\vec{k}'\cdot\delta_i} \underbrace{\left(\frac{1}{\Omega} \sum_{\vec{j}} e^{i(\vec{k}'-\vec{k})\cdot\vec{j}} \right)}_{\delta_{\vec{k}, \vec{k}'}} b_{\vec{k}'}^\dagger a_{\vec{k}} \right) \\
&= -t \sum_{\delta_i} \sum_{\vec{k}, \vec{k}'} \left(e^{i\vec{k}'\cdot\delta_i} \delta_{\vec{k}, \vec{k}'} a_{\vec{k}}^\dagger b_{\vec{k}'} + e^{-i\vec{k}'\cdot\delta_i} \delta_{\vec{k}, \vec{k}'} b_{\vec{k}'}^\dagger a_{\vec{k}} \right) \\
&= -t \sum_{\delta_i} \sum_{\vec{k}} \left(e^{i\vec{k}\cdot\delta_i} a_{\vec{k}}^\dagger b_{\vec{k}} + e^{-i\vec{k}\cdot\delta_i} b_{\vec{k}}^\dagger a_{\vec{k}} \right) \\
&= -t \sum_{\vec{k}} \left(\left(e^{i\vec{k}\cdot\left(-\frac{\sqrt{3}}{2}a\hat{x}-\frac{a}{2}\hat{y}\right)} + e^{i\vec{k}\cdot\left(\frac{\sqrt{3}}{2}a\hat{x}-\frac{a}{2}\hat{y}\right)} + e^{i\vec{k}\cdot(a\hat{y})} \right) a_{\vec{k}}^\dagger b_{\vec{k}} \right. \\
&\quad \left. + \left(e^{-i\vec{k}\cdot\left(-\frac{\sqrt{3}}{2}a\hat{x}-\frac{a}{2}\hat{y}\right)} + e^{-i\vec{k}\cdot\left(\frac{\sqrt{3}}{2}a\hat{x}-\frac{a}{2}\hat{y}\right)} + e^{-i\vec{k}\cdot(a\hat{y})} \right) b_{\vec{k}}^\dagger a_{\vec{k}} \right) \\
&= -t \sum_{\vec{k}} \left(\left(e^{ik_x\cdot\left(-\frac{\sqrt{3}}{2}a\right)} e^{ik_y\left(-\frac{a}{2}\right)} + e^{ik_x\cdot\left(\frac{\sqrt{3}}{2}a\right)} e^{ik_y\left(-\frac{a}{2}\right)} + e^{ik_y a} \right) a_{\vec{k}}^\dagger b_{\vec{k}} \right. \\
&\quad \left. + \left(e^{-ik_x\cdot\left(-\frac{\sqrt{3}}{2}a\right)} e^{-ik_y\left(-\frac{a}{2}\right)} + e^{-ik_x\cdot\left(\frac{\sqrt{3}}{2}a\right)} e^{-ik_y\left(-\frac{a}{2}\right)} + e^{-ik_y a} \right) b_{\vec{k}}^\dagger a_{\vec{k}} \right) \\
&= -t \sum_{\vec{k}} \left(\left(\left(e^{-i\frac{\sqrt{3}k_x a}{2}} + e^{i\frac{\sqrt{3}k_x a}{2}} \right) e^{-i\frac{k_y a}{2}} + e^{ik_y a} \right) a_{\vec{k}}^\dagger b_{\vec{k}} \right. \\
&\quad \left. + \left(\left(e^{-i\frac{\sqrt{3}k_x a}{2}} + e^{i\frac{\sqrt{3}k_x a}{2}} \right) e^{i\frac{k_y a}{2}} + e^{-ik_y a} \right) b_{\vec{k}}^\dagger a_{\vec{k}} \right) \\
&= -t \sum_{\vec{k}} \left(\left(2\cdot\cos\left(\frac{\sqrt{3}}{2}ak_x\right) e^{-i\frac{k_y a}{2}} + e^{ik_y a} \right) a_{\vec{k}}^\dagger b_{\vec{k}} + \left(2\cdot\cos\left(\frac{\sqrt{3}}{2}ak_x\right) e^{i\frac{k_y a}{2}} + e^{-ik_y a} \right) b_{\vec{k}}^\dagger a_{\vec{k}} \right) \\
&= \sum_{\vec{k}} \left(f\left(\vec{k}\right) a_{\vec{k}}^\dagger b_{\vec{k}} + f^*\left(\vec{k}\right) b_{\vec{k}}^\dagger a_{\vec{k}} \right) \quad\quad\quad (2.22)
\end{aligned}
$$

where the sum over $\vec{k}$ runs over the first Brillouin zone and $f\left(\vec{k}\right) = -t \cdot \left(2\cdot\cos\left(\frac{\sqrt{3}}{2}ak_x\right) e^{-i\frac{k_y a}{2}} + e^{ik_y a} \right)$.

In matrix form this becomes

$$H_0\left(\vec{k}\right) = \begin{bmatrix} 0 & f\left(\vec{k}\right) \\ f^*\left(\vec{k}\right) & 0 \end{bmatrix} \tag{2.23}$$

To extract the dispersion relation we need to solve for the eigenvalues of this Hamiltonian, we find that

$$E\left(\vec{k}\right) = \pm\sqrt{f\left(\vec{k}\right)f^*\left(\vec{k}\right)} \tag{2.24}$$

we can visualize this to reveal the band structure. At the corners of the Brillouin zone the valance and conductance band touch each other, meaning that pristine graphene is a zero band gap semimetal. We also call the points where the bands touch each other Dirac points for reasons that will become clear in the next section. To investigate these points further we shall make a low energy expansion of the dispersion relation in Eq. (2.24).
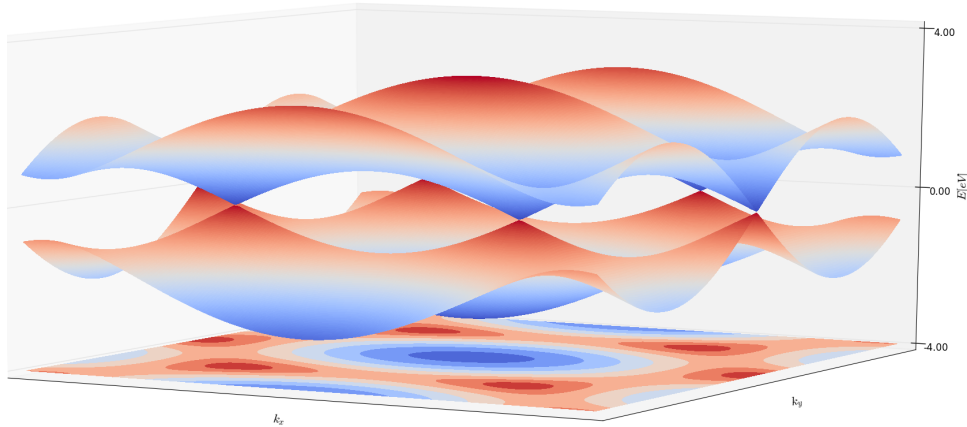
Figure 2.3: The bandstructure of graphene with only nearest neighbour hopping. The six peaks and valleys are called Dirac points and are situated at the corners of the Brillouin zone.

2.4.1 *Low energy expansion of single layer graphene*

We want to investigate the Dirac points we see in the band structure of graphene. To do this we will make a low energy expansion of the dispersion relation in Eq. (2.24). We only need to make an expansion of the function $f(k)$ near the any of the non-equivalent corners in Eq. (2.8) as $\tilde{f}^*(k)$ will be the conjugate of $\tilde{f}(k)$.

The Taylor expansion of $f(k)$ is given by

$$\tilde{f}(k) \approx f\left(\vec{K}\right) + \left.\frac{df\left(\vec{k}\right)}{dk_x}\right|_{\vec{k}=\vec{K}} \cdot k_x + \left.\frac{df\left(\vec{k}\right)}{dk_y}\right|_{\vec{k}=\vec{K}} \cdot k_y + \mathcal{O}\left(\vec{k}^2\right)$$

$$= \left.t \cdot \sqrt{3}a\sin\left(\frac{\sqrt{3}}{2}a \cdot k_x\right)e^{-i\frac{k_y a}{2}}\right|_{\vec{k}=\vec{K}} \cdot k_x + \left.ita \cdot e^{i\frac{k_y}{2}a}\cos\left(\frac{\sqrt{3}}{2}a \cdot k_x\right) + i\right|_{\vec{k}=\vec{K}} \cdot k_y$$

$$= -\frac{3}{2}ta \cdot k_x - \frac{3}{2}ita \cdot k_y \tag{2.25}$$

Then our Hamiltonian becomes

$$\tilde{H}_0\left(\vec{k}\right) = \frac{3}{2}ta\begin{bmatrix} 0 & -k_x - ik_y \\ -k_x + ik_y & 0 \end{bmatrix} \tag{2.26}$$

$$= \begin{bmatrix} 0 & \tilde{f}\left(\vec{k}\right) \\ \tilde{f}^*\left(\vec{k}\right) & 0 \end{bmatrix} \tag{2.27}$$

The Fermi velocity vector is given by

$$\vec{v}_F = \frac{1}{\hbar}\nabla_{\vec{k}}E\left(\vec{k}\right)$$

$$= \pm\frac{3a}{2\hbar}t\begin{bmatrix} \cos(\phi) \\ \sin(\phi) \end{bmatrix} \tag{2.28}$$

because $k_x = k\cos(\phi)$ and $k_y = k\sin(\phi)$ where ϕ is the angle enclosed by $\vec{k}$ and the k_x-axis. The Fermi velocity then becomes

$$v_F = \frac{3a}{2\hbar}t \tag{2.29}$$

If you substitute $k_x = -i\hbar\partial_x$ and $k_y = -i\hbar\partial_y$ in Eq. (2.26) the Hamiltonian can be rewritten as [8]

$$\tilde{H}_0\left(\vec{k}\right) = \hbar v_F\vec{\sigma} \cdot \vec{k} \tag{2.30}$$

where $\vec{\sigma} = (\sigma_x, \sigma_y)$ are the usual Pauli matrices. If we perform the same calculation for the other non-equivalent corner we find

$$\tilde{H}_0\left(\vec{k}\right) = \hbar v_F\vec{\sigma}' \cdot \vec{k} \tag{2.31}$$

where $\vec{\sigma}' = (-\sigma_x, \sigma_y)$.

If we cast Eq. (2.26) into the form

$$\tilde{H}_0\left(\vec{k}\right) = \hbar v_F \left|\vec{k}\right| \begin{bmatrix} 0 & e^{-i\theta_{\vec{k}}} \\ e^{i\theta_{\vec{k}}} & 0 \end{bmatrix} \tag{2.32}$$

its eigenvalues i.e. the energy becomes which is illustrated in Fig. 2.4

$$E\left(\vec{k}\right) = \pm\hbar v_F \left|\vec{k}\right| \tag{2.33}$$

and the eigenvectors for positive energies (quasi-electrons) and negative energies (quasi-holes) are

$$\Psi_{\vec{k}}^{\pm,\vec{K}}\left(\vec{r}\right) = \frac{1}{\sqrt{2}} e^{i\vec{k}\cdot\vec{r}} \begin{bmatrix} e^{-i\frac{\theta_{\vec{k}}}{2}} \\ \pm e^{i\frac{\theta_{\vec{k}}}{2}} \end{bmatrix}$$

where $\theta_{\vec{k}} = \tan^{-1}\left(\frac{k_x}{k_y}\right)$.

Now it has become clear why we refer to the corners of the Brillouin zone as Dirac points. The dispersion relation strongly resembles the Dirac-Weyl equation for massless particles, the difference is that for our quasi-particles the speed of light is replaced by the Fermi velocity v_F which has a value of about $v_F \sim 10^6$ [m/s] (0.003 c) [2]. Another interesting property that becomes apparent is the absence of backscattering for slowly varying impurities. If we compute the matrix element of the backscattering process we find it to be zero

$$\left\langle -\vec{k} \middle| H \middle| \vec{k} \right\rangle = \frac{1}{2A} \int e^{2i\vec{k}\cdot\vec{r}} \begin{bmatrix} e^{i\frac{\theta_{-\vec{k}}}{2}} & e^{-i\frac{\theta_{-\vec{k}}}{2}} \end{bmatrix} \begin{bmatrix} V\left(\vec{r}\right) & 0 \\ 0 & V\left(\vec{r}\right) \end{bmatrix} \begin{bmatrix} e^{-i\frac{\theta_{\vec{k}}}{2}} \\ e^{i\frac{\theta_{\vec{k}}}{2}} \end{bmatrix} d\vec{r}$$

$$= \frac{1}{2A} \int e^{2i\vec{k}\cdot\vec{r}} \left(V e^{i\frac{\Delta\theta_k}{2}} + V e^{-i\frac{\Delta\theta_k}{2}} \right) d\vec{r}$$

$$= \frac{1}{A} \int e^{2i\vec{k}\cdot\vec{r}} \left(V \cos\left(\frac{\Delta\theta_k}{2}\right) \right) d\vec{r}$$

$$= 0$$

where $V\left(\vec{r}\right)$ can be taken constant as it is a slowly varying potential and for backscattering it holds that $\Delta\theta_k = \pi$ and A is the area of the unit cell. This behaviour of the quasi-particles imparts a high electron mobility upon graphene giving it its excellent conducting ability.

Graphene low energy band structure
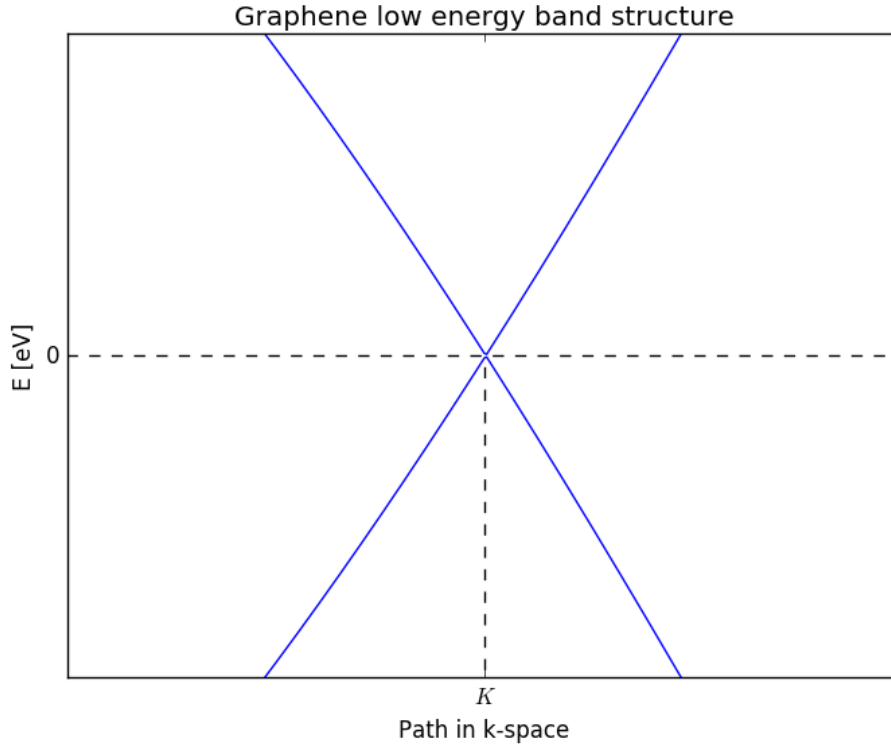
Figure 2.4: Low energy single layer graphene bandstructure. Around the Dirac points we see that the band structure becomes linear and the two bands touch each other. In three dimensions it would look like a cone around the Dirac point.

2.5 BI-LAYER GRAPHENE

Bi-layer graphene is a configuration where two layers of graphene are stacked on top of each other. There exist several configurations of bi-layer graphene, the most common being Bernal (AB) stacked bi-layer graphene where the sublattice A_2 of the second layer lies directly over the sublattice B_1 of the first layer. Another would be AA stacked bi-layer graphene [9] where the A_2 sublattice lies directly above the A_1 sublattice and a configuration where the two layers are rotated relative to each other. We will only focus on the Bernal stacked bi-layer graphene with nearest neighbour hoppings and even though the two layers in bi-layer graphene are separated by a distance $c \approx 3.35\text{Å}$ [10] we treat as if it is still a two dimensional model, then the Hamiltonian becomes

$$H_0^{Bi} = -t \sum_{\langle \vec{j}, \vec{i} \rangle} \sum_{\sigma} \left(a^\dagger_{1,\vec{j},\sigma} b_{1,\vec{i},\sigma} + b^\dagger_{1,\vec{j},\sigma} a_{1,\vec{i},\sigma} \right) - t \sum_{\langle \vec{j}, \vec{i} \rangle} \sum_{\sigma} \left(a^\dagger_{2,\vec{j},\sigma} b_{2,\vec{i},\sigma} + b^\dagger_{2,\vec{j},\sigma} a_{2,\vec{i},\sigma} \right)$$
$$- t_\perp \sum_{\vec{j}} \sum_{\sigma} \left(b^\dagger_{1,\vec{j},\sigma} a_{2,\vec{j},\sigma} + a^\dagger_{2,\vec{j},\sigma} b_{1,\vec{j},\sigma} \right) \tag{2.34}$$

The first term in Eq. 2.34 signifies the intralayer hopping in the first layer, the second term the intralayer hopping in the second layer and the final term the interlayer hopping between the first and the second layer with a hopping amplitude of $t_\perp$. Again because the system is translationally invariant we Fourier transform to momentum space via Eq. (2.20) and (2.21) then just solely focusing on the interlayer hopping term (as the first two terms are exactly as in single layer graphene) we get

$$H_{0,B_1A_2}^{Bi} = -t_\perp \sum_{\vec{j}} \sum_{\sigma} \left(b^\dagger_{1,\vec{j},\sigma} a_{2,\vec{j},\sigma} + a^\dagger_{2,\vec{j},\sigma} b_{1,\vec{j},\sigma} \right)$$

$$= -\frac{t_\perp}{\Omega} \sum_{\vec{j}} \sum_{\vec{k}} \left(e^{-i\vec{k}'\cdot\vec{j}} b^\dagger_{1,\vec{k}'} e^{i\vec{k}\cdot\vec{j}} a_{2,\vec{k}} + e^{-i\vec{k}'\cdot\vec{j}} a^\dagger_{2,\vec{k}'} e^{i\vec{k}\cdot\vec{j}} b_{1,\vec{k}} \right)$$

$$= -\frac{t_\perp}{\Omega} \sum_{\vec{j}} \sum_{\vec{k}} \left(e^{i(\vec{k}'-\vec{k})\cdot\vec{j}} b^\dagger_{\vec{k}'} a_{\vec{k}} + e^{i(\vec{k}'-\vec{k})\cdot\vec{j}} a^\dagger_{2,\vec{k}'} b_{1,\vec{k}} \right)$$

$$= -t_\perp \sum_{\vec{k}} \left(\underbrace{\left(\frac{1}{\Omega} \sum_{\vec{j}} e^{i(\vec{k}-\vec{k}')\cdot\vec{j}} \right)}_{\delta_{\vec{k},\vec{k}'}} b^\dagger_{1,\vec{k}'} a_{2,\vec{k}} + \underbrace{\left(\frac{1}{\Omega} \sum_{\vec{j}} e^{i(\vec{k}-\vec{k}')\cdot\vec{j}} \right)}_{\delta_{\vec{k},\vec{k}'}} a^\dagger_{2,\vec{k}'} b_{1,\vec{k}} \right)$$

$$= -t_\perp \sum_{\vec{k}} \left(b^\dagger_{1,\vec{k}} a_{2,\vec{k}} + a^\dagger_{2,\vec{k}} b_{1,\vec{k}} \right) \tag{2.35}$$

To find the dispersion relation we use the results from single layer graphene and combine them with the interlayer hopping result to put our Hamiltonian in matrix form, whose eigenvalues will yield the dispersion relation of which we will make a low energy expansion as we did in section 2.4.1.

The resulting Hamiltonian matrix is

$$H_0^{Bi}\left(\vec{k}\right) = \begin{bmatrix} 0 & f\left(\vec{k}\right) & 0 & 0 \\ f^*\left(\vec{k}\right) & 0 & -t_\perp & 0 \\ 0 & -t_\perp & 0 & f\left(\vec{k}\right) \\ 0 & 0 & f^*\left(\vec{k}\right) & 0 \end{bmatrix} \tag{2.36}$$

in the basis $\{A_1, B_1, A_2, B_2\}$. The eigenvalues of this matrix i.e. the dispersion relation is given by

$$E(k) = \begin{bmatrix} \frac{1}{2}t_\perp + \frac{1}{2}\sqrt{t_\perp^2 + 4f(\vec{k})\,f^*(\vec{k})} \\ \frac{1}{2}t_\perp - \frac{1}{2}\sqrt{t_\perp^2 + 4f(\vec{k})\,f^*(\vec{k})} \\ -\frac{1}{2}t_\perp + \frac{1}{2}\sqrt{t_\perp^2 + 4f(\vec{k})\,f^*(\vec{k})} \\ -\frac{1}{2}t_\perp - \frac{1}{2}\sqrt{t_\perp^2 + 4f(\vec{k})\,f^*(\vec{k})} \end{bmatrix} \qquad (2.37)$$

In Fig. 2.5 we see a visualisation of this dispersion relation. What is immediately clear is that we now have four energy bands. Of which two are shifted in energy by the interlayer hopping amplitude $t_\perp$.
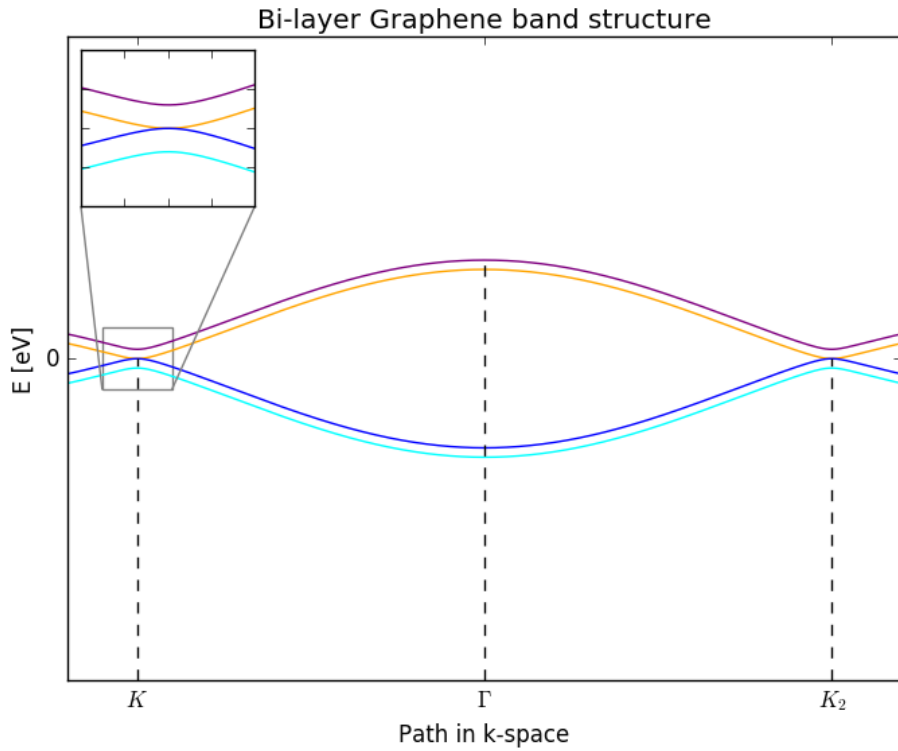
Figure 2.5: Band structure of Bernal stacked bi-layer graphene. Two of the bands touch each other at the Dirac point but we see that the bands have a parabolic nature instead of a linear one as in single layer graphene.

2.5.1 *Low energy expansion of bi-layer graphene*

To make a low energy description of bi-layer graphene we employ a method beside Taylor expanding the functions $f\left(\vec{k}\right)$ and $f^*\left(\vec{k}\right)$ namely we shall assume that the interlayer hopping amplitude $t_\perp$ is large compared to the energy of the system such that $\frac{E}{t_\perp} \ll 1$ and use the property to solve a system of recursive equations to see if we can reduce the Hamiltonian matrix in Eq. (2.36) to a smaller size.

Our system looks like

$$H_0^{Bi} \times \begin{bmatrix} A_1 \\ B_1 \\ A_2 \\ B_2 \end{bmatrix} = E \times \begin{bmatrix} A_1 \\ B_1 \\ A_2 \\ B_2 \end{bmatrix} \tag{2.38}$$

$$\begin{bmatrix} 0 & \tilde{f}\left(\vec{k}\right) & 0 & 0 \\ \tilde{f}^*\left(\vec{k}\right) & 0 & -t_\perp & 0 \\ 0 & -t_\perp & 0 & \tilde{f}\left(\vec{k}\right) \\ 0 & 0 & \tilde{f}^*\left(\vec{k}\right) & 0 \end{bmatrix} \times \begin{bmatrix} A_1 \\ B_1 \\ A_2 \\ B_2 \end{bmatrix} = E \times \begin{bmatrix} A_1 \\ B_1 \\ A_2 \\ B_2 \end{bmatrix} \tag{2.39}$$

which leads to a set of recursive equations which we can solve with the condition set above

$$\tilde{f}\left(\vec{k}\right) B_1 = E A_1 \tag{2.40}$$

$$\tilde{f}^*\left(\vec{k}\right) A_1 - t_\perp A_2 = E B_1 \tag{2.41}$$

$$-t_\perp B_1 + \tilde{f}\left(\vec{k}\right) B_2 = E A_2 \tag{2.42}$$

$$\tilde{f}^*\left(\vec{k}\right) A_2 = E B_2 \tag{2.43}$$

Using Eq. (2.42) we get an expression for A_2

$$A_2 = -\frac{E}{t_\perp} B_1 + \frac{\tilde{f}^*\left(\vec{k}\right)}{t_\perp} A_1 \tag{2.44}$$

substitute this into Eq. (2.42)

$$-t_\perp B_1 + \tilde{f}\left(\vec{k}\right) B_2 = -\frac{E^2}{t_\perp} B_1 + \frac{E \cdot \tilde{f}^*\left(\vec{k}\right)}{t_\perp} A_1$$

$$-t_\perp \left(1 - \frac{E^2}{t_\perp^2}\right) B_1 = \frac{E \cdot \tilde{f}^*\left(\vec{k}\right)}{t_\perp} A_1 - \tilde{f}\left(\vec{k}\right) B_2$$

$$-t_\perp B_1 = -\tilde{f}\left(\vec{k}\right) B_2$$

$$B_1 = \frac{\tilde{f}\left(\vec{k}\right)}{t_\perp} B_2 \tag{2.45}$$

Then we substitute Eq. (2.45) into Eq. (2.40)

$$\frac{\tilde{f}\left(\vec{k}\right)^2}{t_\perp} B_2 = EA_1 \tag{2.46}$$

Using Eq. (2.42) we get an expression for B_1

$$B_1 = -\frac{E}{t_\perp} A_2 + \frac{\tilde{f}\left(\vec{k}\right)}{t_\perp} B_2 \tag{2.47}$$

substitute this into Eq. (2.41)

$$\tilde{f}^*\left(\vec{k}\right) A_1 - t_\perp A_2 = -\frac{E^2}{t_\perp} A_2 + \frac{E \cdot \tilde{f}\left(\vec{k}\right)}{t_\perp} B_2$$

$$-t_\perp \left(1 - \frac{E^2}{t_\perp^2}\right) A_2 = -\tilde{f}^*\left(\vec{k}\right) A_1 + \frac{E \cdot \tilde{f}\left(\vec{k}\right)}{t_\perp} B_2$$

$$-t_\perp A_2 = -\tilde{f}^*\left(\vec{k}\right) A_1$$

$$A_2 = \frac{\tilde{f}^*\left(\vec{k}\right)}{t_\perp} A_1 \tag{2.48}$$

Then we substitute Eq. (2.48) into Eq. (2.43)

$$\frac{\tilde{f}^*\left(\vec{k}\right)^2}{t_\perp} A_1 = EB_2 \tag{2.49}$$

Now we have reduced our Hamiltonian from a 4×4 matrix to a 2×2 matrix in the low energy regime

$$H_0^{Bi} \overset{\frac{E}{t_\perp} \ll 1}{\to} \tilde{H}_0^{Bi} \tag{2.50}$$

$$\begin{bmatrix} 0 & \tilde{f}\left(\vec{k}\right) & 0 & 0 \\ \tilde{f}^*\left(\vec{k}\right) & 0 & -t_\perp & 0 \\ 0 & -t_\perp & 0 & \tilde{f}\left(\vec{k}\right) \\ 0 & 0 & \tilde{f}^*\left(\vec{k}\right) & 0 \end{bmatrix} \overset{\frac{E}{t_\perp} \ll 1}{\to} \begin{bmatrix} 0 & \frac{\tilde{f}(\vec{k})^2}{t_\perp} \\ \frac{\tilde{f}^*(\vec{k})^2}{t_\perp} & 0 \end{bmatrix} \tag{2.51}$$

Our reduced Hamiltonian is much easier to use, its eigenvalues are

$$E\left(k\right) = \pm \frac{\tilde{f}\left(\vec{k}\right)\tilde{f}^*\left(\vec{k}\right)}{t_\perp} \tag{2.52}$$

This dispersion relation is illustrated in Fig. 2.6. If we rewrite our Hamiltonian in the form

$$\begin{aligned} \tilde{H}_0^{Bi} &= \frac{\left(\frac{3ta}{2}\right)^2}{t_\perp} \begin{bmatrix} 0 & (-k_x - ik_y)^2 \\ (-k_x + ik_y)^2 & 0 \end{bmatrix} \\ &= \frac{\hbar^2 v_F^2}{t_\perp} \begin{bmatrix} 0 & (-k_x - ik_y)^2 \\ (-k_x + ik_y)^2 & 0 \end{bmatrix} \\ &= \frac{1}{2m} \begin{bmatrix} 0 & (-k_x - ik_y)^2 \\ (-k_x + ik_y)^2 & 0 \end{bmatrix} \end{aligned} \tag{2.53}$$

where we introduced a parameter $m = \frac{t_\perp}{2\hbar^2 v_F^2}$. Then our Hamiltonian results in a quadratic dispersion relation

$$\tilde{E}\left(k\right) = \frac{|k|^2}{2m} \tag{2.54}$$

resembling a conventional dispersion relation for a semi-conductor.

Our Hamiltonian now describes an effective hopping between non-equivalent sublattices A_1 to B_2 via a transition from B_1 to A_2 where a mass is imparted upon our quasi-particle [11][12].
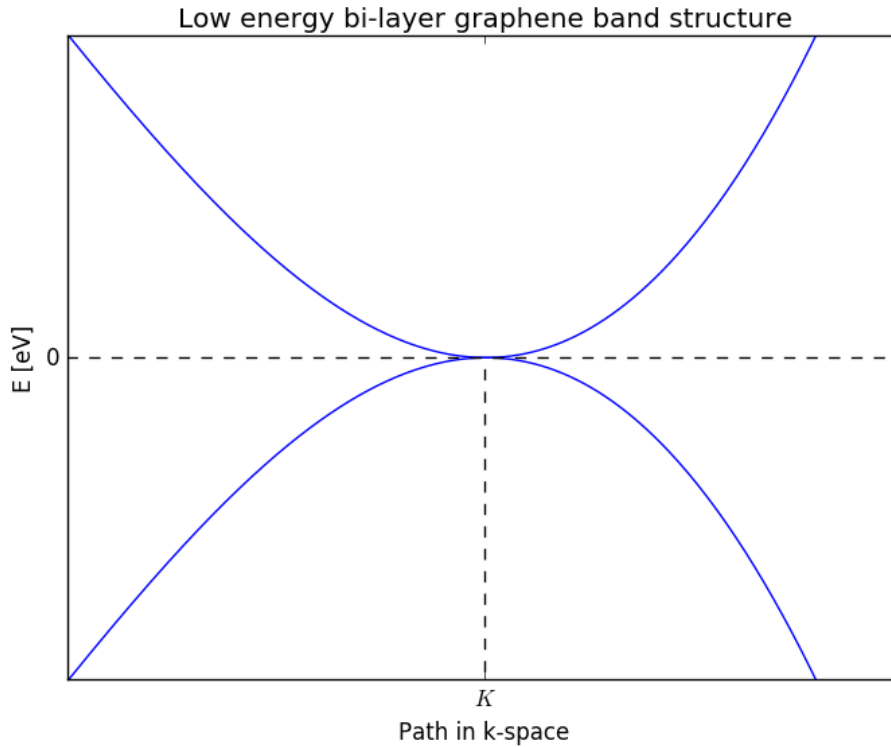
Figure 2.6: The low energy band structure of bi-layer graphene near the Dirac point. We see that two bands have disappeared due to our low energy approximation.

2.6 TRI-LAYER GRAPHENE

Tri-layer graphene is a configuration where three layers of graphene are stacked on top of each other. Like bi-layer graphene several configurations exist but we shall only focus on rhombohedral stacked (ABC) trilayer graphene and Bernal stacked (ABA) trilayer graphene. In ABC stacked tri-layergraphene the sublattice A_2 is directly on top of the sublattice B_1 and A_3 is directly on top of B_2. Whereas in ABA stacked tri-layer graphene the sublattice A_2 is directly on top of sublattice B_1 and the sublattice B_3 is now directly on top of sublattice A_2 illustrated in Fig. 2.7. We will again treat as if tri-layer graphene is a pure two dimensional material neglecting the interlayer spacing.

Figure 2.7: ABA tri-layer graphene on the left and ABC tri-layer on the right. The blue paths indicate the interlayer hopping and the yellow paths indicate intralayer hopping. Image taken from [13].

We first start with the Hamiltonian to describe the system and illustrate the band structure of both stacking configurations then make a low energy expansion as we did for single and bi-layer graphene and discuss the results.

2.6.1 *Rhombohedral (ABC) stacked tri-layer graphene*

The Hamiltonian for ABC stacked tri-layer graphene is given by

$$
H_0^{ABC} = -t \sum_{\langle \vec{j}, \vec{i} \rangle} \sum_{\sigma} \left(a_{1,\vec{j},\sigma}^\dagger b_{1,\vec{i},\sigma} + b_{1,\vec{j},\sigma}^\dagger a_{1,\vec{i},\sigma} \right) - t \sum_{\langle \vec{j}, \vec{i} \rangle} \sum_{\sigma} \left(a_{2,\vec{j},\sigma}^\dagger b_{2,\vec{i},\sigma} + b_{2,\vec{j},\sigma}^\dagger a_{2,\vec{i},\sigma} \right)
$$

$$
- t \sum_{\langle \vec{j}, \vec{i} \rangle} \sum_{\sigma} \left(a_{3,\vec{j},\sigma}^\dagger b_{3,\vec{i},\sigma} + b_{3,\vec{j},\sigma}^\dagger a_{3,\vec{i},\sigma} \right) - t_\perp \sum_{\vec{j}} \sum_{\sigma} \left(b_{1,\vec{j},\sigma}^\dagger a_{2,\vec{j},\sigma} + a_{2,\vec{j},\sigma}^\dagger b_{1,\vec{j},\sigma} \right)
$$

$$
- t_\perp \sum_{\vec{j}} \sum_{\sigma} \left(b_{2,\vec{j},\sigma}^\dagger a_{3,\vec{j},\sigma} + a_{3,\vec{j},\sigma}^\dagger b_{2,\vec{j},\sigma} \right) \tag{2.55}
$$

which in momentum space becomes the matrix (following the method described in the previous sections)

$$
H_0^{ABC}\left(\vec{k}\right) = \begin{bmatrix} 0 & f\left(\vec{k}\right) & 0 & 0 & 0 & 0 \\ f^*\left(\vec{k}\right) & 0 & -t_\perp & 0 & 0 & 0 \\ 0 & -t_\perp & 0 & f\left(\vec{k}\right) & 0 & 0 \\ 0 & 0 & f^*\left(\vec{k}\right) & 0 & -t_\perp & 0 \\ 0 & 0 & 0 & -t_\perp & 0 & f\left(\vec{k}\right) \\ 0 & 0 & 0 & 0 & f^*\left(\vec{k}\right) & 0 \end{bmatrix} \tag{2.56}
$$

its eigenvalues, the dispersion relation, is depicted in Fig 2.8. We notice we have six bands, a pair for each layer in the system.
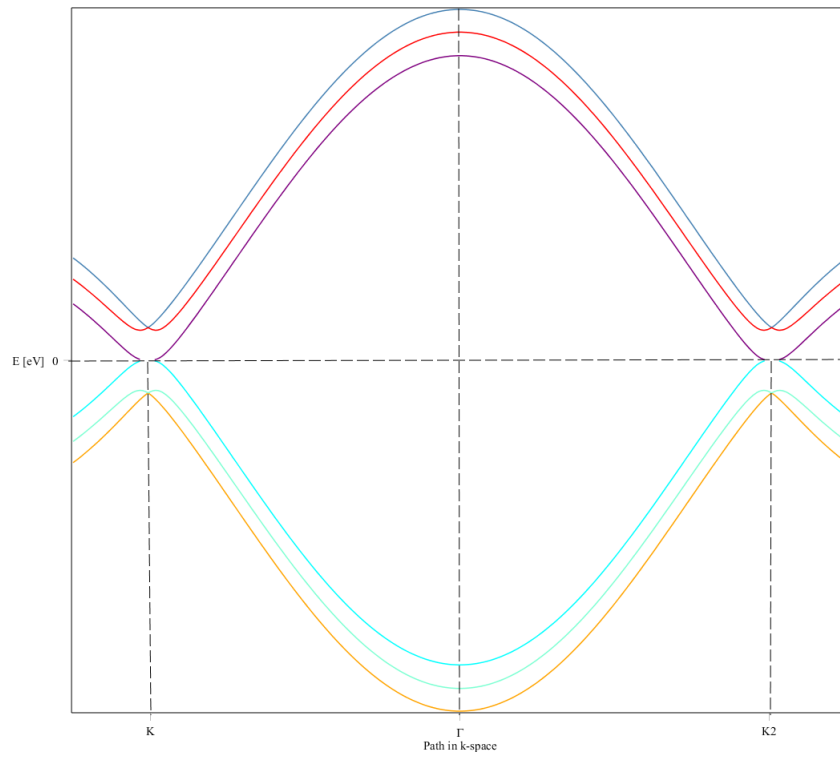
Figure 2.8: Full bandstructure of ABC stacked tri-layer graphene.

2.6.1.1 *Low energy expansion*

To make a low energy expansion of ABC stacked tri-layer graphene we proceed as we did for bi-layer graphene, solving the recursive equations to arrive at a reduced Hamiltonian from which the low energy dispersion relation can be extracted.

$$H_0^{ABC} \times \begin{bmatrix} A_1 \\ B_1 \\ A_2 \\ B_2 \\ A_3 \\ B_3 \end{bmatrix} = E \times \begin{bmatrix} A_1 \\ B_1 \\ A_2 \\ B_2 \\ A_3 \\ B_3 \end{bmatrix} \tag{2.57}$$

$$\begin{bmatrix} 0 & f\left(\vec{k}\right) & 0 & 0 & 0 & 0 \\ f^*\left(\vec{k}\right) & 0 & -t_\perp & 0 & 0 & 0 \\ 0 & -t_\perp & 0 & f\left(\vec{k}\right) & 0 & 0 \\ 0 & 0 & f^*\left(\vec{k}\right) & 0 & -t_\perp & 0 \\ 0 & 0 & 0 & -t_\perp & 0 & f\left(\vec{k}\right) \\ 0 & 0 & 0 & 0 & f^*\left(\vec{k}\right) & 0 \end{bmatrix} \times \begin{bmatrix} A_1 \\ B_1 \\ A_2 \\ B_2 \\ A_3 \\ B_3 \end{bmatrix} = E \times \begin{bmatrix} A_1 \\ B_1 \\ A_2 \\ B_2 \\ A_3 \\ B_3 \end{bmatrix} \tag{2.58}$$

It results in the system of equations

$$f\left(\vec{k}\right) B_1 = EA_1 \tag{2.59}$$

$$f^*\left(\vec{k}\right) A_1 - t_\perp A_2 = EB_1 \tag{2.60}$$

$$-t_\perp B_1 + f\left(\vec{k}\right) B_2 = EA_2 \tag{2.61}$$

$$f^*\left(\vec{k}\right) A_2 - t_\perp A_3 = EB_2 \tag{2.62}$$

$$-t_\perp B_2 + f\left(\vec{k}\right) B_3 = EA_3 \tag{2.63}$$

$$f^*\left(\vec{k}\right) A_3 = EB_3 \tag{2.64}$$

solving the above system leads to

$$\begin{bmatrix} 0 & \frac{f(\vec{k})^3}{t_\perp^2} \\ \frac{f^*(\vec{k})^3}{t_\perp^2} & 0 \end{bmatrix} \times \begin{bmatrix} A_1 \\ B_3 \end{bmatrix} = \begin{bmatrix} EA_1 \\ EB_3 \end{bmatrix} \tag{2.65}$$

with a dispersion relation

$$E\left(\vec{k}\right) = \pm \frac{f\left(\vec{k}\right)^3 f\left(\vec{k}\right)^{*3}}{t_{\perp}^2} \tag{2.66}$$

$$= \pm \frac{v_F^3}{t_{\perp}} |k|^3 \tag{2.67}$$

which is illustrated in Fig. 2.9. There are only two bands left in the low energy description of ABC stacked tri-layer graphene and they cross over each other at the Dirac points.
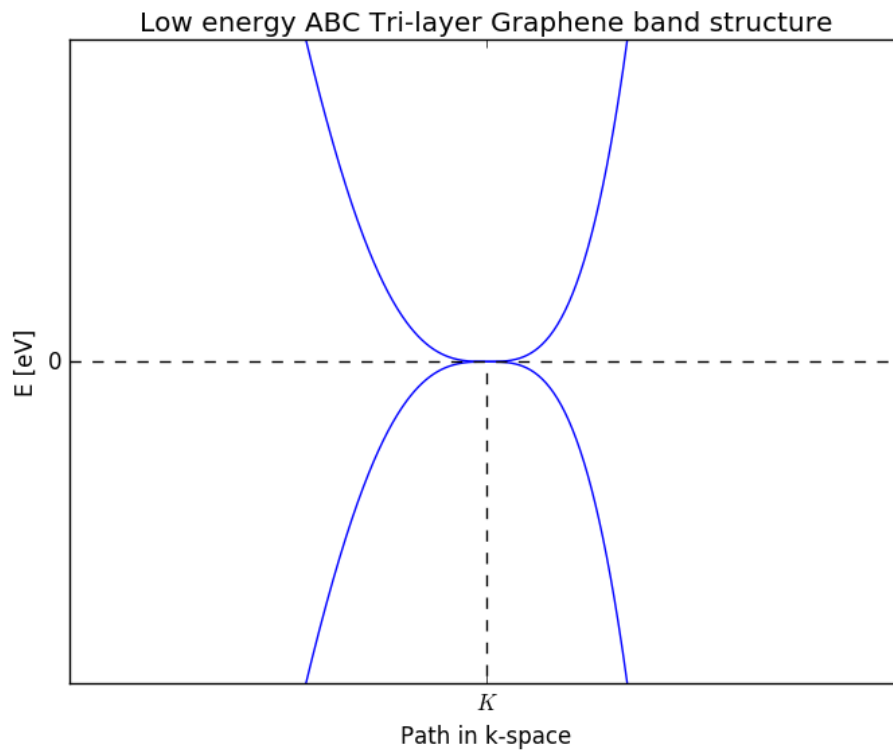
Figure 2.9: Low energy band structure of ABC stacked tri-layer graphene near the Dirac point.

2.6.2 *Bernal (ABA) stacked tri-layer graphene*

The Hamiltonian for ABA stacked tri-layer graphene is given by in

$$
H_0^{ABA} = -t \sum_{\langle \vec{j}, \vec{i} \rangle} \sum_{\sigma} \left(a_{1,\vec{j},\sigma}^\dagger b_{1,\vec{i},\sigma} + b_{1,\vec{j},\sigma}^\dagger a_{1,\vec{i},\sigma} \right) - t \sum_{\langle \vec{j}, \vec{i} \rangle} \sum_{\sigma} \left(a_{2,\vec{j},\sigma}^\dagger b_{2,\vec{i},\sigma} + b_{2,\vec{j},\sigma}^\dagger a_{2,\vec{i},\sigma} \right)
$$

$$
-t \sum_{\langle \vec{j}, \vec{i} \rangle} \sum_{\sigma} \left(a_{3,\vec{j},\sigma}^\dagger b_{3,\vec{i},\sigma} + b_{3,\vec{j},\sigma}^\dagger a_{3,\vec{i},\sigma} \right) - t_\perp \sum_{\vec{j}} \sum_{\sigma} \left(b_{1,\vec{j},\sigma}^\dagger a_{2,\vec{j},\sigma} + a_{2,\vec{j},\sigma}^\dagger b_{1,\vec{j},\sigma} \right)
$$

$$
-t_\perp \sum_{\vec{j}} \sum_{\sigma} \left(a_{2,\vec{j},\sigma}^\dagger b_{3,\vec{j},\sigma} + b_{3,\vec{j},\sigma}^\dagger a_{2,\vec{j},\sigma} \right)
$$

which in momentum space becomes the matrix

$$
H_0^{ABA} \left(\vec{k} \right) =
\begin{bmatrix}
0 & f\left(\vec{k}\right) & 0 & 0 & 0 & 0 \\
f^*\left(\vec{k}\right) & 0 & -t_\perp & 0 & 0 & 0 \\
0 & -t_\perp & 0 & f\left(\vec{k}\right) & 0 & -t_\perp \\
0 & 0 & f^*\left(\vec{k}\right) & 0 & 0 & 0 \\
0 & 0 & 0 & 0 & 0 & f\left(\vec{k}\right) \\
0 & 0 & -t_\perp & 0 & f^*\left(\vec{k}\right) & 0
\end{bmatrix}
\tag{2.68}
$$

Its dispersion relation is illustrated in Fig. 2.10. It becomes clear that in ABA stacked tri-layer graphene there are a total of 6 bands of which two form the Dirac cones we found for single layer graphene and the other four bands are parabolic in nature and thus carry massive particles. Thus ABA stacked tri-layer graphene has both massless relativistic quasi-particles and massive quasi-particles as charge carriers.
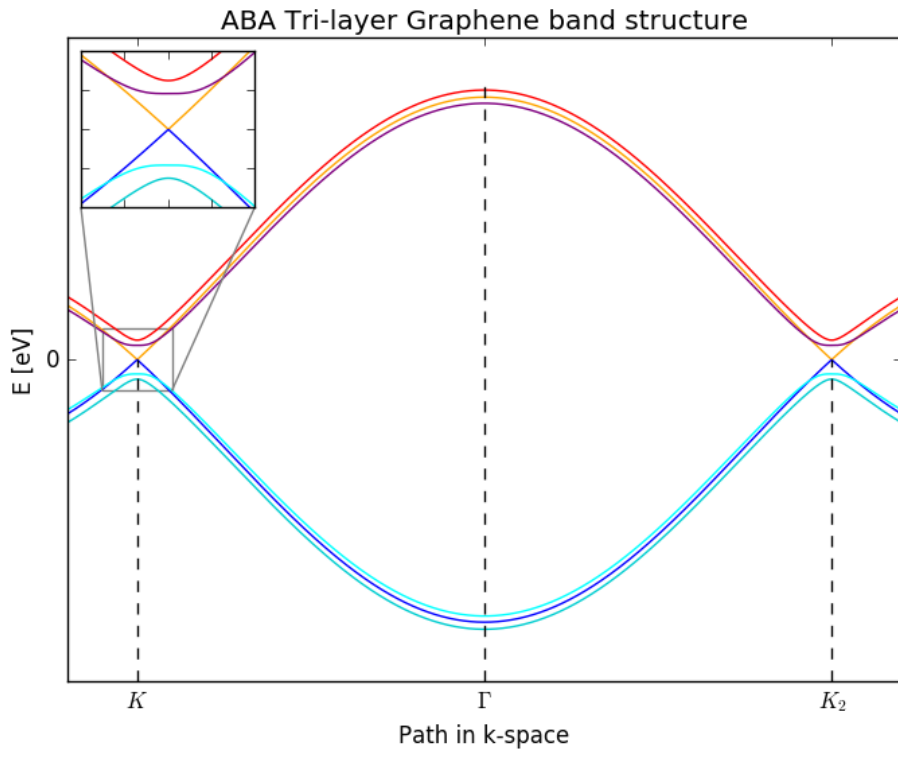
Figure 2.10: ABA stacked trilayer graphene band structure.

2.6.2.1 *Low energy expansion*

To make a low energy expansion of ABA stacked tri-layer graphene we proceed in the exact same way as we did for bi-layer and ABC tri-layer graphene. We need to solve the system of recursive equations based upon the Hamiltonian in Eq. (2.68) which are

$$
H_0^{ABA} \times
\begin{bmatrix}
A_1 \\ B_1 \\ A_2 \\ B_2 \\ A_3 \\ B_3
\end{bmatrix}
= E \times
\begin{bmatrix}
A_1 \\ B_1 \\ A_2 \\ B_2 \\ A_3 \\ B_3
\end{bmatrix}
\tag{2.69}
$$

$$
\begin{bmatrix}
0 & f\left(\vec{k}\right) & 0 & 0 & 0 & 0 \\
f^*\left(\vec{k}\right) & 0 & -t_\perp & 0 & 0 & 0 \\
0 & -t_\perp & 0 & f\left(\vec{k}\right) & 0 & -t_\perp \\
0 & 0 & f^*\left(\vec{k}\right) & 0 & 0 & 0 \\
0 & 0 & 0 & 0 & 0 & f\left(\vec{k}\right) \\
0 & 0 & -t_\perp & 0 & f^*\left(\vec{k}\right) & 0
\end{bmatrix}
\times
\begin{bmatrix}
A_1 \\ B_1 \\ A_2 \\ B_2 \\ A_3 \\ B_3
\end{bmatrix}
= E \times
\begin{bmatrix}
A_1 \\ B_1 \\ A_2 \\ B_2 \\ A_3 \\ B_3
\end{bmatrix}
\tag{2.70}
$$

It results in the system of equations

$$
f\left(\vec{k}\right) B_1 = E A_1
\tag{2.71}
$$

$$
f^*\left(\vec{k}\right) A_1 - t_\perp A_2 = E B_1
\tag{2.72}
$$

$$
-t_\perp B_1 + f\left(\vec{k}\right) B_2 - t_\perp B_3 = E A_2
\tag{2.73}
$$

$$
f^*\left(\vec{k}\right) A_2 = E B_2
\tag{2.74}
$$

$$
f\left(\vec{k}\right) B_3 = E A_3
\tag{2.75}
$$

$$
-t_\perp A_2 + f^*\left(\vec{k}\right) A_3 = E B_3
\tag{2.76}
$$

solving the above system leads to

$$
\begin{bmatrix}
0 & \dfrac{\tilde{f}(\vec{k})^2}{\sqrt{2}t_\perp} & 0 & 0 \\
\dfrac{\tilde{f}^*(\vec{k})^2}{\sqrt{2}t_\perp} & 0 & 0 & 0 \\
0 & 0 & 0 & \tilde{f}\left(\vec{k}\right) \\
0 & 0 & \tilde{f}^*\left(\vec{k}\right) & 0
\end{bmatrix}
\times
\begin{bmatrix}
A_1 + A_3 \\ \sqrt{2}B_2 \\ A_1 - A_3 \\ B_1 - B_3
\end{bmatrix}
=
\begin{bmatrix}
E\left(A_1 + A_3\right) \\ E\left(\sqrt{2}B_2\right) \\ E\left(A_1 - A_3\right) \\ E\left(B_1 - B_3\right)
\end{bmatrix}
\tag{2.77}
$$

with a dispersion relation illustrated in Fig. 2.11

$$E(k) = \begin{bmatrix} \pm \frac{\tilde{f}(\vec{k})\tilde{f}^*(\vec{k})}{\sqrt{2}t_\perp} \\ \pm \sqrt{\tilde{f}\left(\vec{k}\right)\tilde{f}^*\left(\vec{k}\right)} \end{bmatrix} \tag{2.78}$$

$$= \begin{bmatrix} \pm \frac{|\vec{k}|^2}{2\sqrt{2}m} \\ \pm \hbar v_F \left|\vec{k}\right| \end{bmatrix} \tag{2.79}$$

What becomes apparent is that unlike in ABC stacked tri-layer graphene we could only reduce the matrix size to 4×4 instead of 2×2. This means that ABA stacked tri-layer graphene has four bands in the low energy regime. We also see that the orbitals are now a mixture of the lower and upper layer mitigated by sublattice B_2 in the middle layer. Another interesting feature is that all the bands touch now whereas in the high energy regime there was a band gap for the massive quasi-particles.
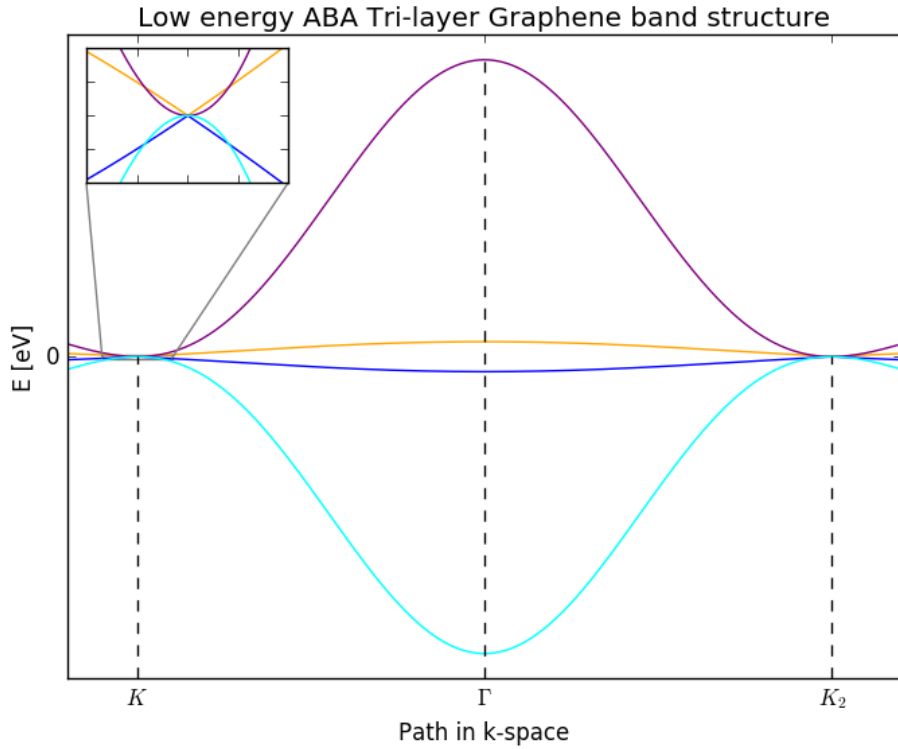

Figure 2.11: Low energy ABA stacked tri-layer graphene. It is important to note that the low energy description is only valid near the Dirac points even though the band structure is plotted for the full path in momentum space is plotted here.

SCATTERING IN ABA TRI-LAYER GRAPHENE

Scattering theory lies at the basis of nearly every physical experiment done at small scale. Free propagation of particles and the difference that results from their interaction results in a lot of information to be gained about the examined system such as transport capabilities.

In this chapter we start with describing the transfer matrix (T-matrix) formalism built upon Green's functions to describe impurity scattering events then we will make a numerical simulation of ABC and ABA stacked tri-layer graphene and compare them to each other.

3.1 T-MATRIX FORMALISM

Many important interactions between particles get treated by perturbation theory. One hopes that the interactions can be treated as a perturbation to the relevant observable i.e. the observable can be expanded in a power series of a small dimensionless parameter. But in many body physics one often encounters that those terms diverge in the higher order and standard perturbation theory isn't very helpful in that case. In 1957 Gell-Mann and Bruckner resolved this issue by summing the divergent terms (an infinite number of them) in the perturbation series before doing the momentum integrals resulting in a well-defined and finite answer [14]. To deal with summing an infinite number of terms a new method was needed which we shall describe in this section.

The retarded single particle Green function for fermions is defined as

$$G^R\left(x, t;\ x', t'\right) = -i\theta\left(t - t'\right)\left\langle\left\{\psi\left(x, t\right), \psi^\dagger\left(x', t'\right)\right\}\right\rangle \tag{3.1}$$

where $\{A, B\}$ stands for the anti-commutator and $x = (\vec{r}, \sigma)$ such that $c^\dagger(x) = c_\sigma^\dagger(\vec{r})$ creates a particle with spin σ at position $\vec{r}$ and $c_\sigma(\vec{r})$ annihilates a particle with a spin σ at position $\vec{r}$. Note that the retarded Green function is only non-zero for $t > t'$ such that effect always follows cause. We can also define an advanced green function

$$G^A\left(x, t;\ x', t'\right) = +i\theta\left(t' - t\right)\left\langle\left\{\psi\left(x, t\right), \psi^\dagger\left(x', t'\right)\right\}\right\rangle \tag{3.2}$$

which is only non-zero for $t < t'$. The Green function represents the probability amplitude for a particle transition from x' at time t' to x at time t, the squared modulus gives the probability of such a transition.

Because we're always dealing with translationally invariant systems i.e. lattices, it is convenient to transform the Green function to the momentum space basis such that it is diagonal in the momentum $\vec{k}$. Consider a basis in momentum space $|\vec{\eta}\rangle = \left|\vec{k}, \sigma\right\rangle$ we may then write[1]

$$
\begin{aligned}
|x\rangle &= \sum_\eta |\eta\rangle \langle \eta \,|\, x\rangle \\
&= \sum_\eta \langle x \,|\, \eta\rangle^* |\eta\rangle \\
&= \sum_\eta \phi_\eta^* (x) |\eta\rangle
\end{aligned}
\tag{3.3}
$$

where $\phi_\eta (x) = \langle x | \eta\rangle$ is the single-particle wavefunction in state $|\eta\rangle$. If we write $\psi^\dagger (x) |0\rangle$ and $|\eta\rangle = c_\eta^\dagger |0\rangle$, where $|0\rangle$ is the vacuum state with no particles in it, we have a relation between the creation operator in the real space basis and the creation operator in the momentum basis

$$
\psi^\dagger (x) = \sum_\eta \phi_\eta^* (x) \, c_\eta^\dagger
\tag{3.4}
$$

and its hermitian conjugate is the annihilation operator

$$
\psi (x) = \sum_\eta \phi_\eta (x) \, c_\eta
\tag{3.5}
$$

Then we can rewrite Eq. (3.4) and Eq. (3.5) to

$$
\begin{aligned}
\psi^\dagger (x) &= \psi_\sigma^\dagger (\vec{r}) \\
&= \sum_{\vec{k}, \sigma} \phi_{\vec{k}, \sigma'}^* (\vec{r}, \sigma) \, c_{\vec{k}, \sigma'}^\dagger \\
&= \sum_{\vec{k}} \phi_{\vec{k}}^* (\vec{r}) \, \delta_{\sigma, \sigma'} c_{\vec{k}, \sigma'}^\dagger \\
&= \sum_{\vec{k}} \phi_{\vec{k}}^* (\vec{r}) \, c_{\vec{k}, \sigma'}^\dagger \\
&= \frac{1}{\sqrt{\Omega}} \sum_{\vec{k}} e^{-i \vec{k} \cdot \vec{r}} c_{\vec{k}, \sigma}^\dagger
\end{aligned}
\tag{3.6}
$$

and for the annihilation operator

$$
\begin{aligned}
\psi_\sigma (\vec{r}) &= \sum_{\vec{k}} \phi_{\vec{k}} (\vec{r}) \, c_{\vec{k}, \sigma} \\
&= \frac{1}{\sqrt{\Omega}} \sum_{\vec{k}} e^{i \vec{k} \cdot \vec{r}} c_{\vec{k}, \sigma}
\end{aligned}
\tag{3.7}
$$

---

1 This actually holds for any basis η but we explicitly used the momentum basis here.

Where we took our particles to live on a flat surface with area Ω with periodic boundary conditions. Using this we can also transform our Green functions to the momentum basis

$$
\begin{aligned}
G^R \left(x, t; \ x', t' \right) &= -i\theta \left(t - t' \right) \left\langle \left\{ \psi \left(x, t \right), \psi^\dagger \left(x', t' \right) \right\} \right\rangle \\
&= -i\theta \left(t - t' \right) \sum_{\eta, \eta'} \phi_\eta \left(x \right) \phi^*_{\eta'} \left(x' \right) \left\langle \left\{ c_\eta \left(t \right), c_\eta^\dagger \left(t' \right) \right\} \right\rangle \\
&= \sum_{\eta, \eta'} \phi_\eta \left(x \right) \phi^*_{\eta'} \left(x' \right) G^R \left(\eta, t; \eta', t' \right) \\
&= \frac{1}{\Omega} \sum_{\vec{k}, \vec{k}'} e^{i\vec{k} \cdot \vec{r}} e^{-i\vec{k}' \cdot \vec{r}'} G^R \left(\vec{k}, \sigma, t; \ \vec{k}', \sigma', t' \right) \\
&= \frac{1}{\Omega} \sum_{\vec{k}, \vec{k}'} e^{i\vec{k} \cdot \left(\vec{r} - \vec{r}' \right)} e^{-i\left(\vec{k} - \vec{k}' \right) \cdot \vec{r}'} G^R \left(\vec{k}, \sigma, t; \ \vec{k}', \sigma', t' \right) \\
&= \frac{1}{\Omega} \sum_{\vec{k}, \vec{k}'} e^{i\vec{k} \cdot \left(\vec{r} - \vec{r}' \right)} e^{-i\left(\vec{k} - \vec{k}' \right) \cdot \vec{r}'} \delta_{\vec{k}, \vec{k}'} G^R \left(\vec{k}, \sigma, t; \ \sigma', t' \right) \\
&= \frac{1}{\Omega} \sum_{\vec{k}} e^{i\vec{k} \cdot \left(\vec{r} - \vec{r}' \right)} G^R \left(\vec{k}, \sigma, t; \ \sigma', t' \right)
\end{aligned}
\tag{3.8}
$$

with the single-particle retarded Green function in momentum space

$$
G^R \left(\eta, t; \eta', t' \right) = -i\theta \left(t - t' \right) \left\langle \left\{ c_\eta \left(t \right), c_\eta^\dagger \left(t' \right) \right\} \right\rangle
\tag{3.9}
$$

$$
G^R \left(\vec{k}, \sigma, t; \ \sigma', t' \right) = -i\theta \left(t - t' \right) \left\langle \left\{ c_{\vec{k}, \sigma} \left(t \right), c_{\vec{k}, \sigma}^\dagger \left(t' \right) \right\} \right\rangle
\tag{3.10}
$$

Note that because in translationally invariant systems the Green functions only depend on the difference between the positions $\vec{r}$ and $\vec{r}'$ such that the Green function in momentum space is only non-zero when $\vec{k} = \vec{k}'$ so $G^R \left(\vec{k}, \sigma, t; \ \vec{k}', \sigma', t' \right) = \delta_{\vec{k}, \vec{k}'} G^R \left(\vec{k}, \sigma, t; \ \sigma', t' \right)$.

We see that the Green function acts as a propagator for particles, it creates a particle (in this case a fermion) at position $\vec{r}$ and annihilates that particle at position $\vec{r}'$ in real space and in momentum space a particle with momentum $\vec{k}$ is created and annihilated with momentum $\vec{k}'$ and for translationally invariant systems we have momentum conservation.

It is convenient to define the unperturbed Green function G_0 as

$$
G_0 \left(\vec{k}, \omega \right) = \lim_{\epsilon \to 0} \frac{1}{\left[\omega \mathbf{I} - H \left(k \right) + i\epsilon \right]}
\tag{3.11}
$$

where the term $i\epsilon$ is added to make the Green function convergent. If we now define a state as

$$
\left| \psi_{\text{new}} \right\rangle = \left| \psi_0 \right\rangle + G_0 V \left| \psi_{\text{old}} \right\rangle
\tag{3.12}
$$

where V is the scattering potential, and iterate this an infinite number of times we get

$$|\psi\rangle = (1 + G_0 V + G_0 V G_0 V + G_0 V G_0 V G_0 V + \ldots)|\psi_0\rangle \tag{3.13}$$

$$\psi(\vec{r}) = \psi_0(\vec{r}) + \int G_0(\vec{r}, \vec{r}') V(\vec{r}') \psi_0(\vec{r}') \, dV + \int G_0(\vec{r}, \vec{r}') V(\vec{r}') G_0(\vec{r}, \vec{r}') V(\vec{r}'') \psi_0(\vec{r}'') \, dV' dV'' + \ldots \tag{3.14}$$

Eq. (3.13) is known as the Born series. The integral of this gives us the probability amplitude of the particle making it to the detector after scattering a number of times. So the first term means that the particle didn't scatter and freely propagated to the detector, the second term means the particle scattered once, the third means the particle scattered twice before hitting the detector and so on. The integral also makes sure that all possible combinations of scattering are taken into account.

Now we define a scattered state as

$$|\psi_s\rangle = |\psi\rangle - |\psi_0\rangle \tag{3.15}$$

such that Eq. (3.13) becomes

$$\begin{aligned} |\psi_s\rangle &= (G_0 V + G_0 V G_0 V + G_0 V G_0 V G_0 V + \ldots)|\psi_0\rangle \\ &= G_0 T |\psi_0\rangle \end{aligned} \tag{3.16}$$

where T is given by

$$T = V(1 - V \cdot G_0)^{-1}$$

$$T(\omega) = V\left(\mathbf{I} - V \cdot \int G_0\left(\vec{k}, \omega\right) d\vec{k}\right)^{-1} \tag{3.17}$$

$T(\omega)$ is called the transfer matrix or T-matrix for short and where $\mathbf{I}$ is the identity matrix. It encodes all scattering events into a single matrix. With this we calculate the local density of states (LDOS) which will reveal quantum modulations induced by the impurity.

The perturbed Green function at an energy ω, describing the presence of an impurity, is given by

$$G(\vec{r}, \vec{r}', \omega) = G_0(\vec{r} - \vec{r}', \omega) + G_0(\vec{r}, \omega) T(\omega) G_0(-\vec{r}', \omega) \tag{3.18}$$

The LDOS is then given by the imaginary part of the trace of the perturbed Green function

$$\rho(\vec{r}, \omega) = -\frac{1}{\pi} \mathrm{Im}\left[\mathrm{Tr}\left(G(\vec{r}, \vec{r}', \omega)\right)\right] \tag{3.19}$$

and in momentum space this becomes

$$\rho(\vec{q}, \omega) = \frac{i}{2\pi} \mathrm{Tr}\left(\int_{BZ} G\left(\vec{k} + \vec{q}, \vec{k}, \omega\right) - G^*\left(\vec{k}, \vec{k} + \vec{q}, \omega\right) d\vec{k}\right) \tag{3.20}$$

note that q is not restricted to the Brillouin zone. But we're not actually interested in the full LDOS but rather the correction to the LDOS of the unperturbed system so

$$\delta G\left(\vec{r},\vec{r}',\omega\right) = G_0\left(\vec{r},\omega\right) T\left(\omega\right) G_0\left(-\vec{r}',\omega\right) \tag{3.21}$$

then the correction LDOS is

$$\delta\rho\left(\vec{r},\omega\right) = -\frac{1}{\pi}\text{Im}\left[\text{Tr}\left(\delta G\left(\vec{r},\vec{r}',\omega\right)\right)\right] \tag{3.22}$$

3.2 IMPURITY SCATTERING IN TRI-LAYER GRAPHENE

In Fig. 3.1 and Fig. 3.2 the real space modulations of the LDOS are given. We observe a three fold symmetry around the impurity for ABC stacked tri-layer graphene. The term $i\epsilon$ that we added to the Green function to make it convergent represents the inverse lifetime of the particle. We chose $\epsilon = 0.05$ here and the interlayer hopping amplitude $t_\perp = 0.3 \cdot t$ for an energy $\omega = 0.038 \cdot t$. We also note that the magnitude on the opposite surface is about ten times smaller than on the surface where the impurity is located.
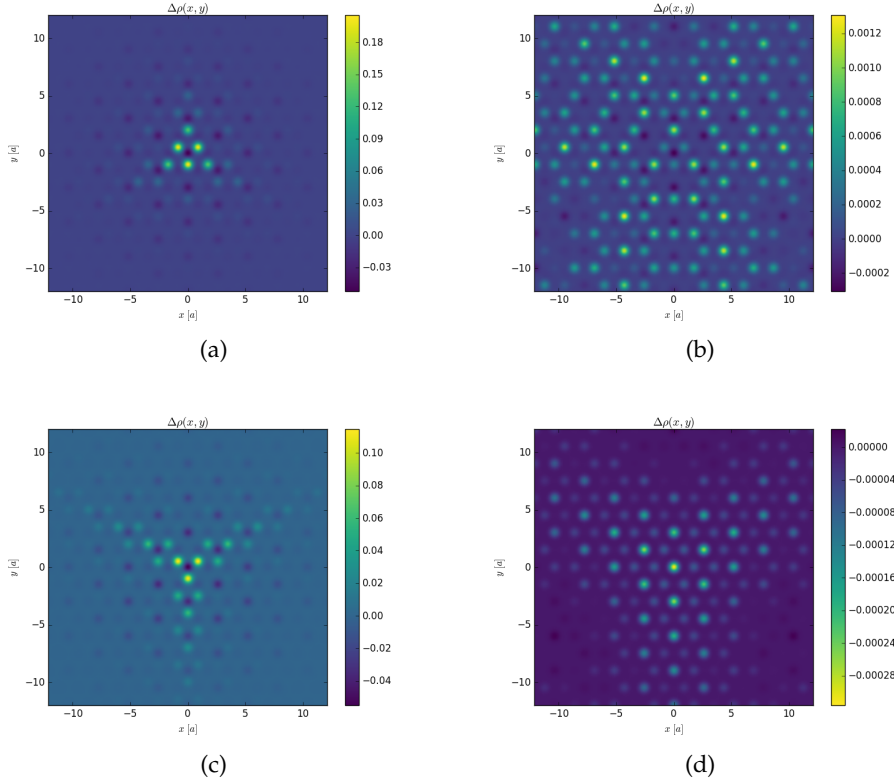
Figure 3.1: Real space modulations in the LDOS in ABC tri-layer stacked graphene ($N = 3$). In the left column we have respectively the LDOS on the bottom surface (i.e. the surface with sublattices A_1 and B_1) with the impurity on A_1 and B_1 and in the right column we have the opposite surface. The magnitude of the impurity is many times larger than the intralayer hopping term $V_0 \gg t$. The energy is $\omega = 0.038 \cdot t$ and the inverse of the particle life time is $\epsilon = 0.05$.

For ABA stacked tri-layer graphene the results are displayed in Fig. 3.2. We see that on the bottom surface with the impurity on A_1 ABA stacked tri-layer graphene does not look different from ABC stacked tri-layer graphene but on the opposite surface we now have a six fold symmetry instead of a three fold symmetry due to the different stacking configuration. If the impurity is on the B_1 sublattice we again recover a three fold symmetry for the bottom surface but have the same six fold symmetry on the top surface albeit a lower magnitude.
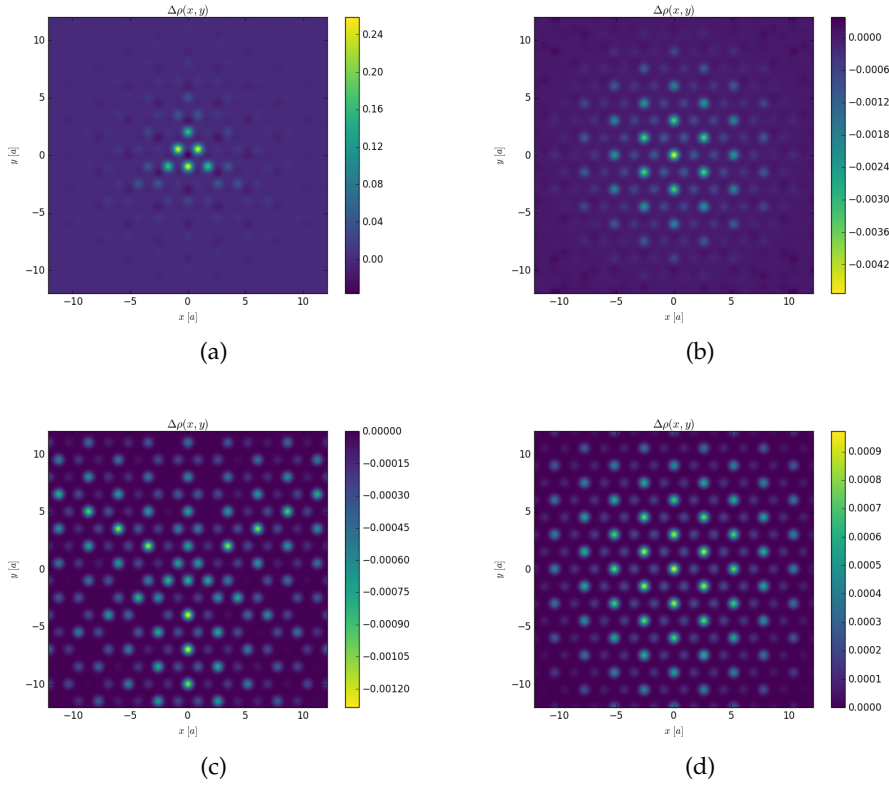
Figure 3.2: Real space modulations in the LDOS in ABA tri-layer stacked graphene ($N = 3$). In the left column we have respectively the LDOS on the bottom surface (i.e. the surface with sublattices A_1 and B_1) with the impurity on A_1 and B_1 and in the right column we have the opposite surface. The magnitude of the impurity is many times larger than the intralayer hopping term $V_0 \gg t$. The energy is $\omega = 0.038 \cdot t$ and the inverse of the particle life time is $\epsilon = 0.05$.

3.2.1 *Friedel oscillations*

Friedel oscillations are the result of the interaction between the impurity and the electrons in the bulk. A presence of a single impurity imparts oscillations in the electron density relating to the Fermi wave vector k_F. Friedel oscillations are a crucial part in the process of explaining transport phenomena such as doping and can be observed directly in STM measurements.

For tri-layer graphene the Green function at low energy can be evaluated as[7][2]

$$\tilde{G}_0^{ABC}\left(\vec{K}_{m,n}^{\zeta} + \vec{q}, \omega\right) \simeq \frac{1}{\omega^2 - q^{2N}} \begin{bmatrix} \omega & -\left(\zeta q e^{i\theta_{mn}^{\zeta}(\vec{q})}\right)^N \\ -\left(\zeta q e^{-i\theta_{mn}^{\zeta}(\vec{q})}\right)^N & \omega \end{bmatrix} \tag{3.23}$$

$$= \frac{1}{\omega^2 - q^6} \begin{bmatrix} \omega & \zeta^3 q^3 e^{3i\theta_{mn}^{\zeta}(\vec{q})} \\ \zeta^3 q^3 e^{-3i\theta_{mn}^{\zeta}(\vec{q})} & \omega \end{bmatrix} \tag{3.24}$$

The off-diagonal components introduce a phase which describes the momentum dependence of the Bloch spinors near the valleys K_{mn}^{ζ} where $\zeta = \pm 1$ indicates the non-equivalent corners and the diagonal components depend on the momentum through the dispersion relation. The real space representation of the Green function is then related to Eq. (3.24) via a Fourier transform

$$G_0\left(\vec{r}, \omega\right) = \frac{1}{n_{BZ}} \sum_{m,n,\zeta} e^{i\vec{K}_{mn}^{\zeta} \cdot \vec{r}} \int_{\mathbb{R}^2} G_0\left(\vec{K}_{m,n}^{\zeta} + \vec{q}, \omega\right) e^{i\vec{q} \cdot \vec{r}} \frac{d^2 q}{4\pi^2} \tag{3.25}$$

where n_{BZ} is the number of unit cells in momentum space which we shall neglect from here onward for convenience and the term $\sum_{mn} = 1$. Then it follows from Eq. (3.21) the large distance diagonal components of Eq. (3.25) are

$$\delta G_{A_1 A_1}\left(\vec{r}, \vec{r}', \omega\right) = G_{0,A_1 A_1}\left(\vec{r}, \omega\right) t\left(\omega\right) G_{0,A_1 A_1}\left(-\vec{r}, \omega\right)$$

$$= -\frac{t\left(\omega\right)}{144 \cdot \omega^{\frac{2}{3}}} \left(H_0\left(\omega^{\frac{1}{3}} r\right)\right)^2 \sum_{\delta m, \delta n} \sum_{\zeta, \zeta'} \cos\left(\Delta \vec{K} \cdot \vec{r}\right) \tag{3.26}$$

and

$$\delta G_{B_3 B_3}\left(\vec{r}, \vec{r}', \omega\right) = G_{0,B_3 A_1}\left(\vec{r}, \omega\right) t\left(\omega\right) G_{0,A_1 B_3}\left(-\vec{r}, \omega\right)$$

$$= -\frac{t\left(\omega\right)}{144 \cdot \omega^{\frac{2}{3}}} \left(-iH_3\left(\omega^{\frac{1}{3}} r\right)\right)^2 \sum_{\delta m, \delta n} \sum_{\zeta, \zeta'} \left(\zeta\zeta'\right)^3 \cos\left(\Delta \vec{K} \cdot \vec{r} - 3\Delta\theta\left(\vec{r}\right)\right) \tag{3.27}$$

where $\Delta\vec{K} = K_{mn}^{\zeta} - K_{m'n'}^{\zeta'}$ and $\Delta\theta\left(\vec{r}\right) = \theta_{mn}^{\zeta}\left(\vec{r}\right) - \theta_{m'n'}^{\zeta'}$ and we introduced the element of the T-matrix as $t\left(\omega\right)$. The function $H_0\left(\omega^{\frac{1}{3}} r\right)$ refers to the first order Hankel function of

---

[2] Note that an analytical expression of the Green function does not always exist. If the orbitals are not fully localized the Green function has no analytical form[15]. In our case the orbitals have a negligible extent so an analytical expression for the Green function exists.

the first kind and $H_3\left(\omega^{\frac{1}{3}}r\right)$ refers to the third order Hankel function of the first kind. In the limit of $\omega^{\frac{1}{3}}r \gg 1$ we can approximate the Hankel functions we then get

$$\delta\rho_{A_1}\left(\vec{r},\omega\right) = -\frac{1}{\pi}\mathrm{Im}\left[i\cdot\frac{t\left(\omega\right)}{144\cdot\omega}\cdot\frac{e^{2i\omega^{\frac{1}{3}}r}}{r}\cos\left(\Delta\vec{K}\cdot\vec{r}\right)\left(1-\frac{i}{4}\frac{1}{\omega^{\frac{1}{3}}r}+\ldots\right)\right] \tag{3.28}$$

$$\delta\rho_{B_3}\left(\vec{r},\omega\right) = -\frac{1}{\pi}\mathrm{Im}\left[i\cdot\frac{t\left(\omega\right)}{144\cdot\omega}\cdot\frac{e^{2i\omega^{\frac{1}{3}}r}}{r}\cos\left(\Delta\vec{K}\cdot\vec{r}-3\Delta\theta\left(\vec{r}\right)\right)\cdot\left(\zeta\zeta'\right)^3\left(1+\frac{35i}{4}\frac{1}{\omega^{\frac{1}{3}}r}+\ldots\right)\right] \tag{3.29}$$

We see that the LDOS decays with $\frac{1}{r}$. When there's an odd number of stacked layers the LDOS of sublattice B_N and A_1 are in anti-phase which means that the sum of the two vanishes and we would have to consider the next leading order leading to a $\frac{1}{r^2}$ decay. This does not happen unless the sublattices B_N and A_1 belong to the same surface, which is only the case for monolayer graphene. We can repeat this calculation for ABA tri-layer graphene and we would find the same dependence on r as we did for ABC tri-layer graphene. As the Green matrix for ABA tri-layer in the low energy regime is given by

$$\tilde{G}_0^{ABA}\left(\vec{K}_{m,n}^{\zeta}+\vec{q},\omega\right) = \begin{bmatrix} \frac{\omega}{\omega^2-q^4} & -\frac{\zeta^2 e^{2i\theta_{mn}^{\pm}(\vec{q})}q^2}{\omega^2-q^4} & 0 & 0 \\ -\frac{\zeta^2 e^{-2i\theta_{mn}^{\pm}(\vec{q})}q^2}{\omega^2-q^4} & \frac{\omega}{\omega^2-q^4} & 0 & 0 \\ 0 & 0 & \frac{\omega}{\omega^2-q^2} & -\frac{\zeta e^{i\theta_{mn}^{\pm}(\vec{q})}q}{\omega^2-q^2} \\ 0 & 0 & -\frac{\zeta e^{-i\theta_{mn}^{\pm}(\vec{q})}q}{\omega^2-q^2} & \frac{\omega}{\omega^2-q^2} \end{bmatrix}$$

$$= \begin{bmatrix} G_0^{ABC,N=2} & 0 \\ 0 & G_0^{ABC,N=1} \end{bmatrix} \tag{3.30}$$

This is also seen by comparing Fig. 3.2 and Fig. 3.1 aside from different shapes of the response in the LDOS, the decay is similar.

3.2.2 *Momentum space LDOS*

In Fig. 3.3 we see the LDOS in momentum space for ABA tri-layer graphene. If the impurity is located at sublattice A_1 the LDOS for sublattices A_1 and A_3 don't elicit a response and are zero, if the impurity is located at sublattice B_1 then the sublattices B_1 and B_3 are zero. One thing that becomes clear when comparing the different locations of the impurity is that the response is the same on the bottom (A_1/B_1) surface. We also note that around the corners of the Brillouin zone we see a two fold symmetric response whereas at the origin we have three fold symmetric response (this is better illustrated in Fig. 3.4). Furthermore the response at the corners and origin for the sublattice B_3 is mirrored in the k_x axis relative to the sublattice A_3
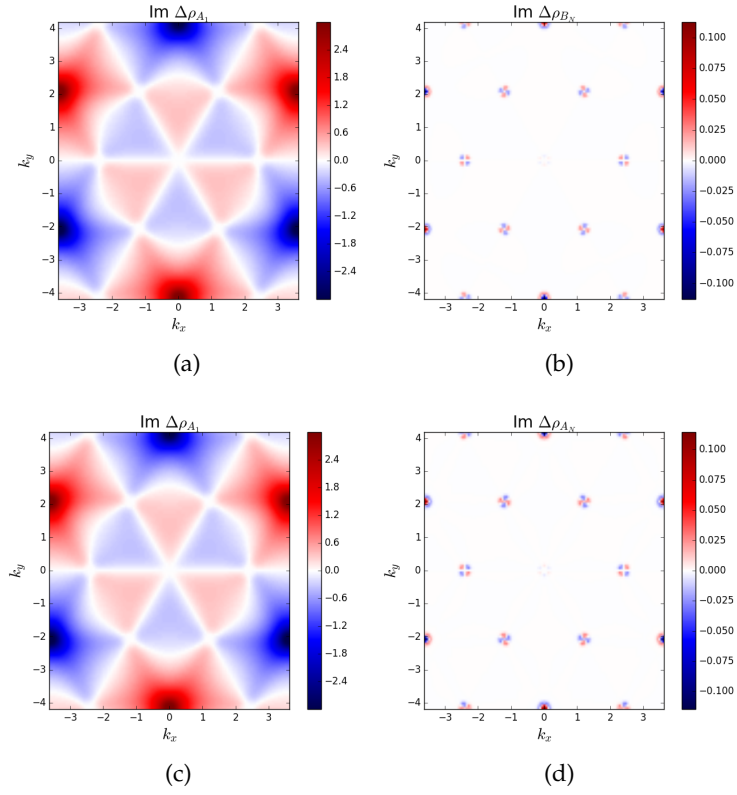
(a)

(b)

(c)

(d)

Figure 3.3: The LDOS in momentum space for ABA tri-layer graphene. In the top row the impurity is located on sublattice A_1 and in the bottom row the impurity is located at sublattice B_1. We chose the energy to be $\omega = 0.038 \cdot t$ and the inverse particle life time $\epsilon = 0.03$ furthermore the impurity potential strength is $v = \frac{1}{\omega}$ and $N = 3$.
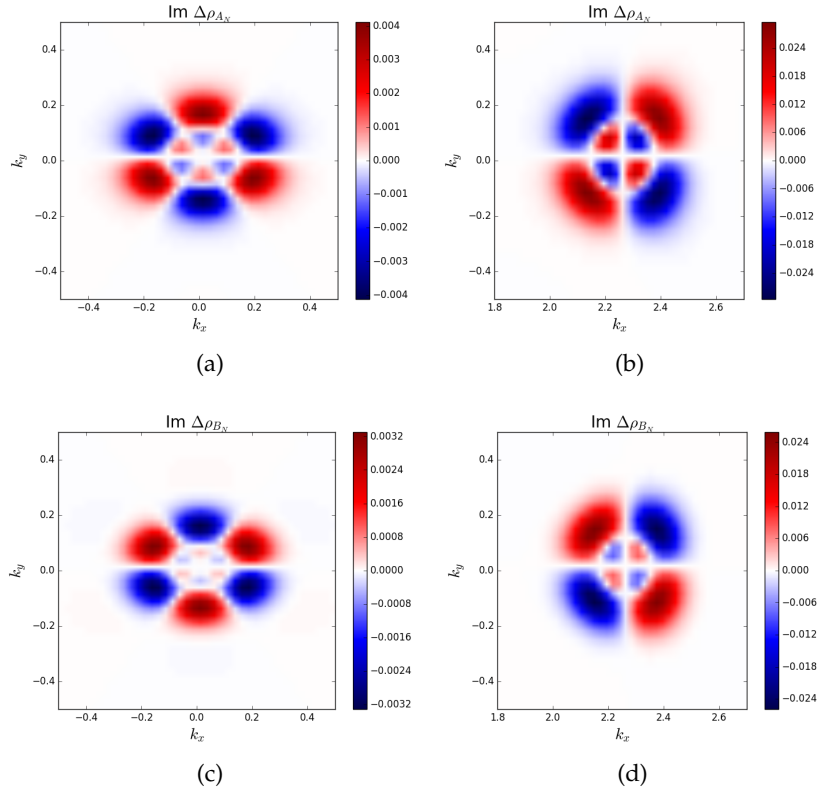
Figure 3.4: Zoom of the points Γ and K respectively for ABA tri-layer graphene. The top row corresponds to the impurity being on sublattice A_1 and the bottom row corresponds to the impurity being on sublattice B_1 and $N = 3$.

Comparing this to the response for ABC tri-layer in Fig. 3.5 we see an immediate difference. In ABC stacked tri-layer graphene the response at the sublattice A_3 for an impurity located at A_1 is not zero but the sublattice A_1 has no response when the impurity is located at A_1 and the sublattice B_1 has no response when the impurity is located at the sublattice B_1. We see a four fold symmetry around the corners of the Brillouin zone while on the sublattice B_3 the response has a six fold symmetry around the corners of the Brillouin zone.

When the impurity is located at the sublattice B_1 we find a two fold symmetry around the corners of the Brillouin zone for the response on sublattice A_3 while on the sublattice B_3 we have a six fold symmetry. Also note the similarity to ABA stacked tri-layer graphene that the response at the origin and the corners are mirrored in the k_x axis.
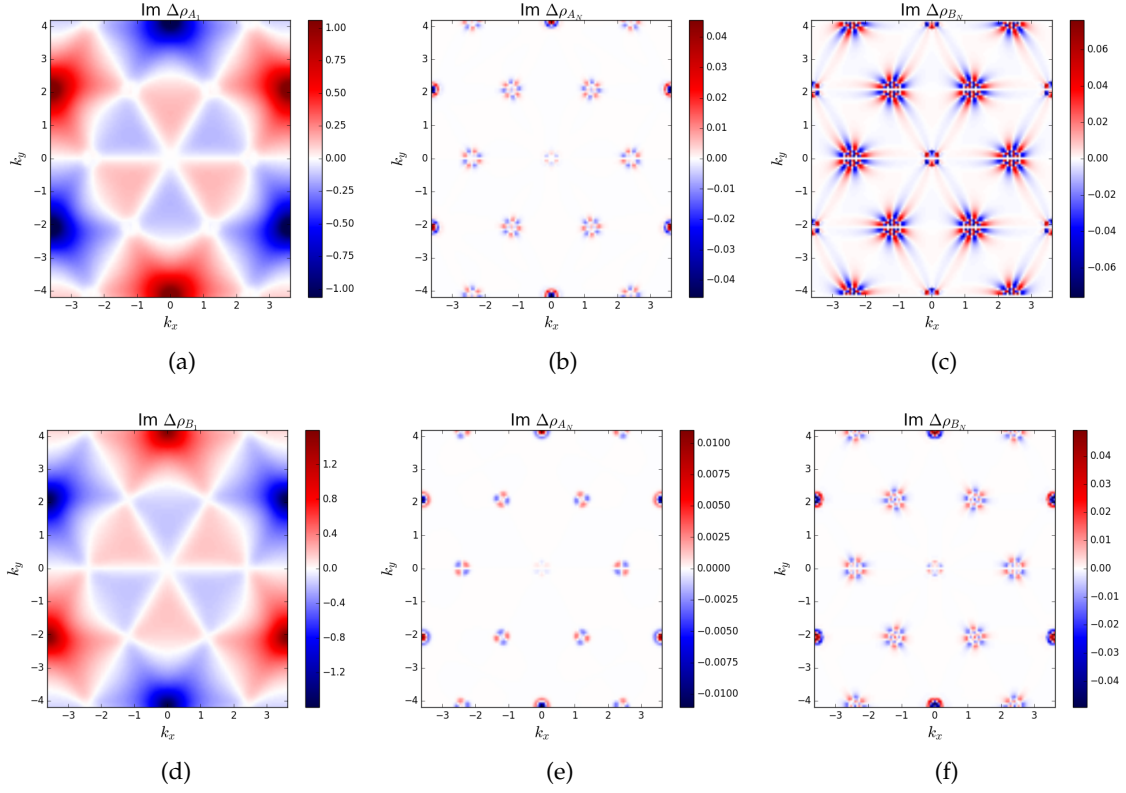
Figure 3.5: The LDOS in momentum space for ABC tri-layer graphene. In the top row the impurity is located on sublattice A_1 except for the first image where it is located on the sublattice B_1 and in the bottom row the impurity is located at sublattice B_1 except for the first image where it is located on the sublattice A_1. We chose the energy to be $\omega = 0.038 \cdot t$ and the inverse particle life time $\epsilon = 0.03$ furthermore the impurity potential strength is $v = \frac{1}{\omega}$ and $N = 3$.
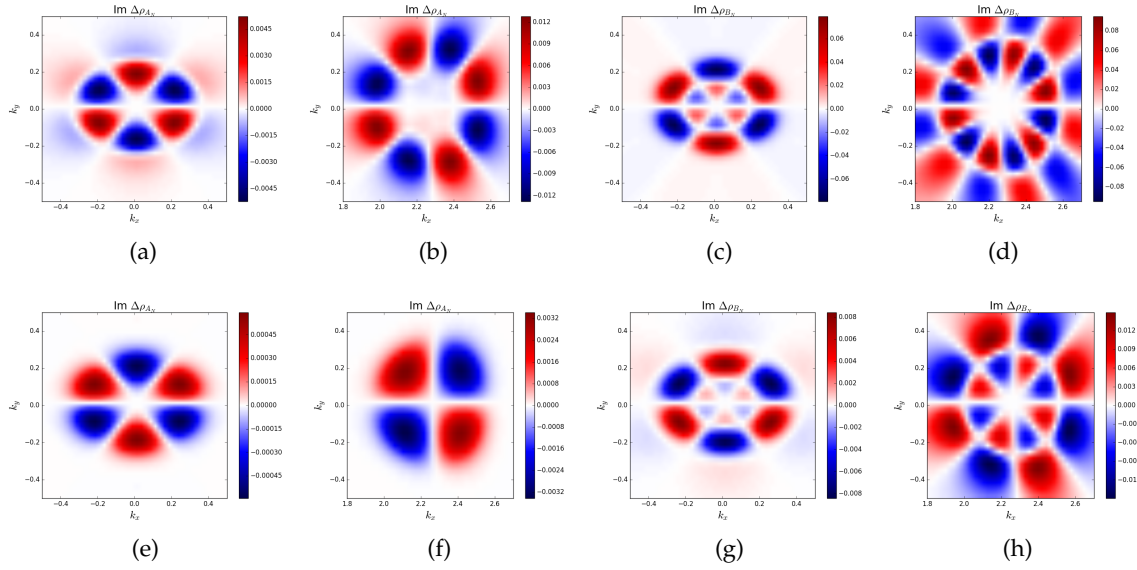
Figure 3.6: Zoom of the points Γ and K respectively on the sublattices A_3 and B_3 for ABC tri-layer graphene. The top row corresponds to the impurity being on sublattice A_1 and the bottom row corresponds to the impurity being on sublattice B_1 and $N = 3$. Figure a, b, e and f depict the response on sublattice A_3 and figure c, d, g and h depict the response on sublattice B_3.

Another interesting thing to look at is when we put the impurity on the sublattice B_2 in tri-layer graphene. The sublattice B_2 lies directly in the center of the honeycomb in ABA stacked tri-layer graphene and can therefore be experimentally probed. We note that the response on the sublattices A_1 and A_3 are the same as well as the response on the sublattices B_1 and B_3 this is because ABA stacked tri-layer graphene is symmetric in both directions thus if we put an impurity in the middle layer the response will be symmetric in both directions.
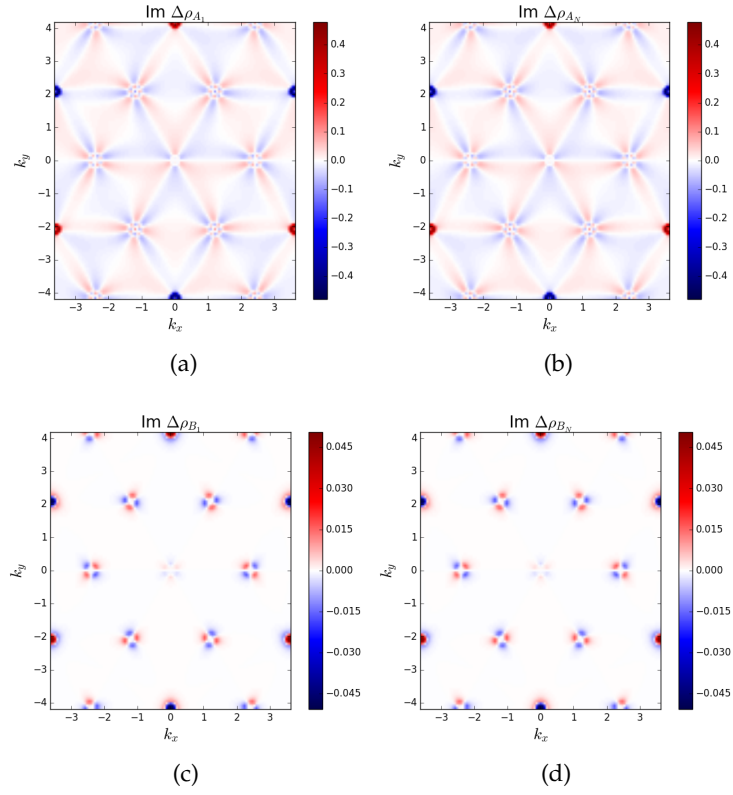
Figure 3.7: The LDOS in momentum space for ABA tri-layer graphene with the impurity located on sublattice B_2. We chose the energy to be $\omega = 0.038 \cdot t$ and the inverse particle life time $\epsilon = 0.03$ furthermore the impurity potential strength is $\nu = \frac{1}{\omega}$ and $N = 3$.
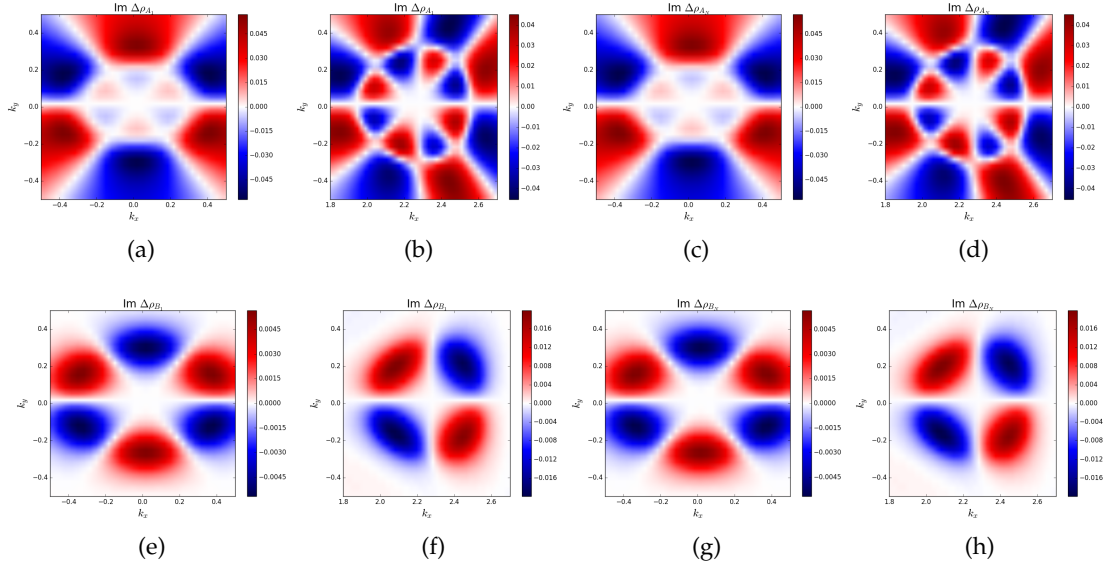
Figure 3.8: Zooms of the points Γ and K respectively for ABA tri-layer graphene with the impurity on the sublattice B_2. The first two images in each row correspond either to A_1 (top row) or B_1 (bottom row) and the last two images correspond to A_3 (top row) and B_3 (bottom row). We chose the energy to be $\omega = 0.038 \cdot t$ and the inverse particle life time $\epsilon = 0.03$ furthermore the impurity potential strength is $v = \frac{1}{\omega}$ and $N = 3$.

CONCLUSIONS

We started with the low energy description of various stackings of graphene where we found that in the low energy regime we reduce the band structure to a low energy band structure with less bands due to the interlayer hopping amplitude being large and thus the stacked layers being harder to reach. We identified that in the case of monolayer graphene we have massless Dirac fermions that have a constant velocity $v_\mathsf{F} = \frac{3}{2}t\alpha$ and in bi-layer and ABC tri-layer we have massive fermions due to the dispersion relation depending on k^2 like a conventional semi-conductor. However in ABA tri-layer graphene we found that we have both massless dirac fermions and massive fermions due to it only being able to be reduced to a four band model around the Dirac points from a six band model.

We addressed elastic scattering in tri-layer graphene through a localized impurity on the outer surfaces and in the case of ABA stacked tri-layer graphene also on the sublattice B_2. The impurity induces Friedel oscillations that decay with $\frac{1}{r}$. This decay does not depend on the magnitude of the potential or the layer upon which the impurity is located. When looking at the momentum space interference patterns we found that ABA tri-layer graphene has less rotational symmetry than ABC tri-layer graphene and also does not elicit a response on both sublattices on the opposing surface due to the Hamiltonian only being able to be reduced to a 4×4 matrix instead of a 2×2 matrix as in ABC tri-layer graphene. Thus by imaging the LDOS we can clearly distinguish between ABA tri-layer graphene and ABC tri-layer graphene.

4.1 FURTHER RESEARCH

Possibilities for further research are simulating the modulus and phase of the momentum space LDOS. These should reveal the Berry phase and the band structure and are interesting from an experimental point of view as one can directly image these in specific cases. The model can also be expanded by allowing hoppings to next-nearest neighbours and allowing for interactions between electrons and also allowing for multiple impurities to be present within or on the surface of the system. The system won't be solvable in an analytical way anymore when its expanded with the previously listed but is still accessible numerically and should provide interesting insights in various properties of multi-layer graphene.

BIBLIOGRAPHY

[1] K. S. Novoselov. "Electric Field Effect in Atomically Thin Carbon Films." In: *Science* 306.5696 (Oct. 2004), pp. 666–669. DOI: 10.1126/science.1102896. URL: http://dx.doi.org/10.1126/science.1102896 (cit. on p. 1).

[2] P. R. Wallace. "The Band Theory of Graphite." In: *Phys. Rev.* 71.9 (May 1947), pp. 622–634. DOI: 10.1103/physrev.71.622. URL: http://dx.doi.org/10.1103/PhysRev.71.622 (cit. on pp. 1, 11).

[3] A. Fasolino, J. H. Los, and M. I. Katsnelson. "Intrinsic ripples in graphene." In: *Nature Materials* 6.11 (Sept. 2007), pp. 858–861. DOI: 10.1038/nmat2011. URL: http://dx.doi.org/10.1038/nmat2011 (cit. on p. 1).

[4] K. S. Novoselov, A. K. Geim, S. V. Morozov, D. Jiang, M. I. Katsnelson, I. V. Grigorieva, S. V. Dubonos, and A. A. Firsov. "Two-dimensional gas of massless Dirac fermions in graphene." In: *Nature* 438.7065 (Nov. 2005), pp. 197–200. DOI: 10.1038/nature04233. URL: http://dx.doi.org/10.1038/nature04233 (cit. on p. 1).

[5] Yuanbo Zhang, Yan-Wen Tan, Horst L. Stormer, and Philip Kim. "Experimental observation of the quantum Hall effect and Berry's phase in graphene." In: *Nature* 438.7065 (Nov. 2005), pp. 201–204. DOI: 10.1038/nature04235. URL: http://dx.doi.org/10.1038/nature04235 (cit. on p. 1).

[6] N. Mermin Neil W. Ashcroft. *Solid State Physics*. Cengage Learning, Inc, Jan. 2, 1976. 848 Seiten. URL: http://www.ebook.de/de/product/3237015/neil_w_ashcroft_n_mermin_solid_state_physics.html (cit. on p. 3).

[7] C. Dutreix and M. I. Katsnelson. "Friedel oscillations at the surfaces of rhombohedral N-layer graphene." In: *Phys. Rev. B* 93.3 (Jan. 2016). DOI: 10.1103/physrevb.93.035413. URL: http://dx.doi.org/10.1103/PhysRevB.93.035413 (cit. on pp. 4, 34).

[8] A. H. Castro Neto, F. Guinea, N. M. R. Peres, K. S. Novoselov, and A. K. Geim. "The electronic properties of graphene." In: *Reviews of Modern Physics* 81.1 (Jan. 2009), pp. 109–162. DOI: 10.1103/revmodphys.81.109. URL: http://dx.doi.org/10.1103/RevModPhys.81.109 (cit. on pp. 6, 10).

[9] Zheng Liu, Kazu Suenaga, Peter J. F. Harris, and Sumio Iijima. "Open and Closed Edges of Graphene Layers." In: *Phys. Rev. Lett.* 102.1 (Jan. 2009). DOI: 10.1103/physrevlett.102.015501. URL: http://dx.doi.org/10.1103/physrevlett.102.015501 (cit. on p. 12).

[10] Pierre Delhaes. *Graphite and precursors*. Vol. 1. CRC Press, 2000 (cit. on p. 12).

[11] Edward McCann and Vladimir I. Fal'ko. "Landau-Level Degeneracy and Quantum Hall Effect in a Graphite Bilayer." In: *Phys. Rev. Lett.* 96.8 (Mar. 2006). DOI: 10.1103/physrevlett.96.086805. URL: http://dx.doi.org/10.1103/PhysRevLett.96.086805 (cit. on p. 17).

[12] Edward McCann and Mikito Koshino. "The electronic properties of bilayer graphene." In: *Rep. Prog. Phys.* 76.5 (Apr. 2013), p. 056503. DOI: 10.1088/0034-4885/76/5/056503. URL: http://dx.doi.org/10.1088/0034-4885/76/5/056503 (cit. on p. 17).

[13] Chun Hung Lui, Zhiqiang Li, Kin Fai Mak, Emmanuele Cappelluti, and Tony F. Heinz. "Observation of an electrically tunable band gap in trilayer graphene." In: *Nat Phys* 7.12 (Sept. 2011), pp. 944–947. DOI: 10.1038/nphys2102. URL: http://dx.doi.org/10.1038/nphys2102 (cit. on p. 19).

[14] Murray Gell-Mann and Keith A. Brueckner. "Correlation Energy of an Electron Gas at High Density." In: *Phys. Rev.* 106.2 (Apr. 1957), pp. 364–368. DOI: 10.1103/physrev.106.364. URL: http://dx.doi.org/10.1103/PhysRev.106.364 (cit. on p. 27).

[15] Cristina Bena. "Green's functions and impurity scattering in graphene." In: *Phys. Rev. B* 79.12 (Mar. 2009). DOI: 10.1103/physrevb.79.125427. URL: http://dx.doi.org/10.1103/PhysRevB.79.125427 (cit. on p. 34).